THE PENNSYLVANIA STATE UNIVERSITY
SCHREYER HONORS COLLEGE

DEPARTMENT OF BIOENGINEERING

MECHANISM AND KINETICS OF HUMAN KINESIN-5 MOTOR PROTEIN

TIFFANY L. SENKOW
SUMMER 2013

A thesis
submitted in partial fulfillment
of the requirements
for a baccalaureate degree in Bioengineering
with honors in Bioengineering

Reviewed and approved* by the following:

William Hancock
Professor of Bioengineering
Thesis Supervisor

Peter Butler
Associate Professor of Bioengineering
Honors Adviser

* Signatures are on file in the Schreyer Honors College.

ABSTRACT

Kinesin-5 (kin-5) is a minimally processive motor protein that walks along antiparallel microtubules to separate the two poles of the mitotic spindle and pull apart chromosomes during mitosis. With the discovery of an inhibitor molecule, kin-5 is a target for antimitotic drugs for cancer treatment; however, compared to conventional kinesin, little is known about kin-5's chemomechanical cycle and mechanism of stepping. It was found that engineered kin-5 motors with a shortened neck linker domain, which undergoes the primary conformational change in each step, exhibit substantially higher processivity, similar to that of conventional kinesin. To better characterize the effects of the length of the neck linker domain, published rates were simulated in the consensus kin-5 chemomechanical pathway and alternate pathways that included combinations of gating, strain-dependent rates, and a novel pathway involving hydrolysis following tethered-head attachment. Kinetics assays were performed to determine the microtubule dissociation rates of kin-5 in different nucleotide states to help rule out or support the proposed pathways. The nucleotide-free and ATP-bound states were confirmed to be strongly-bound to the microtubule, thus rejecting the alternate hydrolysis pathway. Simulations failed to account for the effects on processivity from shortening the neck linker domain.

TABLE OF CONTENTS

LIST OF FIGURES

LIST OF TABLES

ACKNOWLEDGEMENTS

I would like to thank Dr. Hancock for giving me the opportunity to join his lab and for supporting me throughout the year. He believed in my research abilities and encouraged me to continue even when the odds (and mostly timeline) were against me. He demonstrated great patience in answering my numerous questions and walking me through the theory behind nearly all of the new computational and experimental techniques I came across. It is very likely that, without his willingness to accept me into this group, I would not be graduating with honors and may have second guessed going directly to graduate school, so I am incredibly grateful to him.

I would also like to thank Dr. Michael Campbell. When I started at Penn State Behrend, he gladly accepted me into his molecular biology lab where I had my first taste of academic research. There, I learned the basic laboratory and research techniques that formed the cornerstone of my experimental abilities and understanding. His suggestions and guidance shaped me into a more organized and logical researcher.

The research skills I learned in Dr. Craig Cameron's biochemistry lab are invaluable to me. He taught me to pay close attention to the details and constantly reevaluate my assumptions. Thanks to him and his lab group, I also learned the importance of asking for clarification on an advanced concept or for help with troubleshooting.

I would like to thank Dr. Janna Maranas for the opportunity to try my hand at computational protein studies. She welcomed me into her research group where I was exposed to multiple simulation techniques. I would especially like to thank María Antonieta Sánchez Farrán for being a great friend, guiding me, and spending so much time teaching me everything from opening an account in the clusters to efficiently writing bash scripts.

Last summer, I had the pleasure of working with Dr. Thomas West and Jessica Peterson at the University of South Dakota. They taught me how to focus on designing experiments

necessary to prove a hypothesis. While my project was out of my general interest area and I had little experience in microbiology, Dr. West gave me the freedom to truly make it *my* project. I am sure that experience will be vital in helping me succeed in graduate school.

Lastly, by certainly not least, I would like to thank Dave Arginteanu, Yalei Chen, and Niraja Suresh for helping me with the molecular biology and kinetics experiments and Nathan Deffenbaugh for helping me debug my codes. Without Dave and Yalei, I would have had a very boring project and little to no experimental data!

Chapter 1

Introduction to Kinesins

Kinesin motor proteins walk along microtubule filaments in the plus-end direction to control cellular tasks such as cargo transport and spindle organization [1, 2, 3]. There are 45 different kinesin genes in the superfamily in humans, comprising 14 families, categorized by structure and function; each family has a distinct intracellular function [2, 1]. The kinesins are the largest mammalian protein superfamily to have been studied *in silico* and *in vivo*, responsible for a wide variety of intracellular tasks including transporting organelles, protein complexes, and mRNAs to specific destinations and regulating chromosomal and mitotic spindle movements during mitosis and meiosis [2]. Most cells contain multiple different motor proteins within the kinesin superfamily to efficiently accomplish the wide variety of cellular tasks required for survival and replication [2].

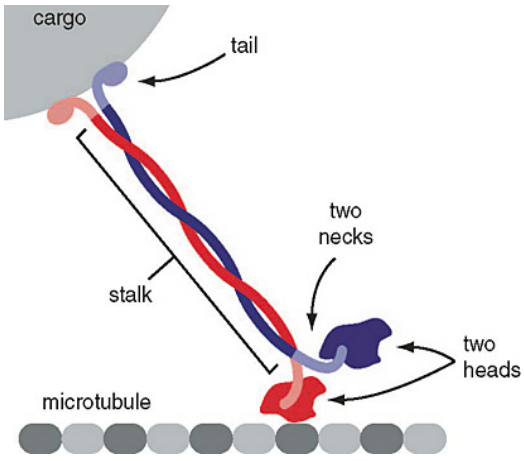

Figure 1: Structure of conventional kinesin-1

The structure of kinesin-1 consists of two heads with neck linker domains, a stalk, and a tail. The heads walk along microtubules, and the tail bind to cargo. Image adapted from [50].

There are three domains: head, stalk, and tail, as shown in Figure 1. The catalytic core, called the head, is located near the N-terminus, involved in

hydrolysis, and is connected to a neck-linker [2, 4]. Conventional kinesin, called kinesin-1 (kin-1), contains two, identical heads that bind to microtubules and adenosine triphosphate (ATP). The neck linkers are then connected to a coiled-coil domain [4]. In kinesin-1, the coiled-coil leads to a cargo-binding domain, while other molecules, such as kinesin-5, the coiled-coil binds to another set of heads to form a tetramer. The combination of the head domain the neck linker domain is referred to as the "motor domain" [2].

The neck linker domain, specific to kinesin families, plays a major role in the mechanics of motility and regulation of activity. It creates the structural transition for stepping via docking to the core motor domain and has entropic spring properties that allow the head to diffuse to the net binding site. The rotation resulting from neck linker docking positions the tethered head forward to step in the forward (plus-end) direction [5, 6]. The neck linker also transmits the intermolecular forces between the heads when they are both bound to the microtubule [6].

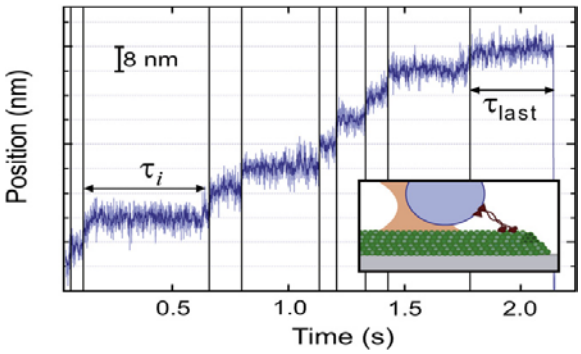

Figure 2: Optical trap measurements of kinesin stepping

Using an optical trap with a glass bead connected to the kinesin, the change in position can be calculated. This method was used to determine the 8 nm step size of kinesin. Image from [16].

KINESIN WALKING AND PROCESSIVITY

Kinesin molecular motors walk possessively along microtubules in the plus-end direction [1, 7, 5, 8, 9]. Microtubules are 25 nm tube-like structures composed of α,β-

tubulin heterodimers spaced 8.2 nm apart in thirteen linear protofilaments, arranged with a polarity with a rapidly-growing plus end and a slowly-growing minus end. [10, 11]. Optical trap experiments measured the kinesin step size as approximately 8 nm, verifying the walks along tubulin dimers [12]. Stepping involves the two heads alternating between high and low affinity states while keeping their hydrolysis cycles in rhythm to ensure at least one head is bound at all times [8, 12, 13]. The ATP-bound and no nucleotide-bound (apo) states bind tightly to the microtubule; the ADP-bound and ADP-P_i states exhibit low affinity [14, 8].

The chemo-mechanical cycle of "conventional" kinesin, referring to kinesin-1, is shown in Figure 3. The cycle shows the consensus of transition states involved with stepping, however, the change

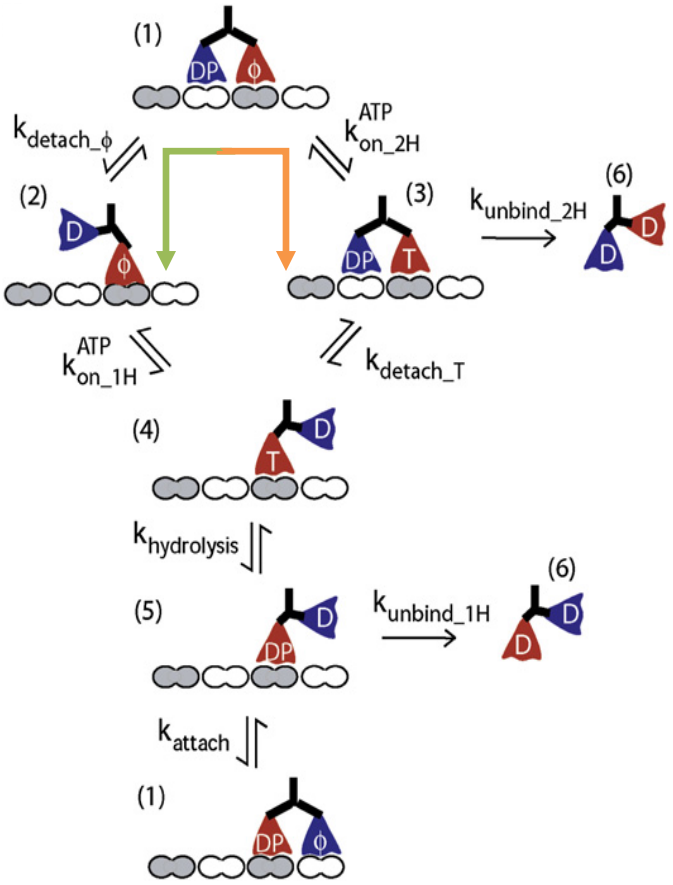

Figure 3: Chemo-mechanical cycle of kinesin-1

This model of the kinesin-1 stepping cycle illustrates processivity in six distinct states. Both front and rear head gating are possible routes. The green arrow shows front-head gating, and the orange rear-head gating. Image adapted from reference [12].

in the neck linker orientation (before state 4) is not included [6, 15, 12, 8]. Starting with both heads attached firmly to microtubules, one head, A, has an ADP and an inorganic phosphate bound and the other head, B, has no nucleotide bound. A loses its phosphate and detaches, although the timing and order is controversial. An ATP binds to head B, making it more strongly bound to the microtubule and driving the conformational change in the neck linker domain, called docking, that moves head A toward the plus-end of the microtubule [12]. It is ATP attachment rather than hydrolysis that promotes the principle conformational change [6]. ATP hydrolysis occurs on head B, so the head then has an ADP with P_i. Head A reattaches to a new tubulin dimer and the ADP releases. The cycle repeats with head B detaching and moving to a new tubulin dimer in the plus-end direction [14]. Both heads can detach from the microtubule if the ATP-bound head is hydrolyzed too quickly and creates a weakly-bound ADP-P_i or ADP state before the second head can attach in a strongly-bound state [16]. This can occur before or after the conformational change in the neck linker [14].

Communication between the heads during stepping is regulated by front-head and/or rear-head gating (this refers to gating *of* a head and not *by* a head). When both heads are bound to the microtubule, interhead tension develops in the neck linker domain. In front-head gating, highlighted by the green arrow in Figure 3, the tension suppresses ATP binding until the rear head detaches to relieve the internal tension on the neck linker [5, 8, 17]. In rear-head gating, highlighted by an orange arrow in Figure 3, the mechanical release from the rear head is accelerated

by the tension, with ATP binding occurring after the dissociation of the rear head from the microtubule [5, 12, 6, 8, 17]. Tension from neck linker docking or a force applied by an optical trap are sufficient to open the "gate" that permits rear-head detachment [18].

Backstepping is a rare event that occurs when the kinesin moves toward the minus end of the microtubule, yet the reasoning and mechanism remains controversial [5, 6, 19]. Carter and Cross found that the transition times between forward and backward steps are inversely proportional to the ATP concentration, which suggests that ATP binding, though not necessarily hydrolysis, is required for backstepping [15]. Hackney also suggested that backsteps are not likely a simple reversal of the chemo-mechanical cycle based on the energy in ATP hydrolysis [19].

Processivity is defined as the number of steps per microtubule interaction before the kinesin completely dissociates [7, 1]. Processivity can also be explained as the number of ATP molecules that are hydrolyzed per motor per interaction with a microtubule [20]. Processive motors bind to microtubules and take multiple steps; minimally processive motors bind, may take a few steps, then dissociate; nonprocessive motors release from the microtubule after each hydrolysis cycle.

A measurement of processivity is the duty ratio, which is the fraction of strongly bound motor protein during the ATPase cycle [21, 22]. Since kinesin-1 has one strongly bound at all times, the duty ratio is nearly one. For a kinesin monomer, the minimum duty ratio is 0.5 [22]. The duty ratio of skeletal muscle myosin is

about 0.05 [23, 24]. Processive motors generally have duty ratios greater than 0.5 [21].

For transporting cargo throughout the cell, a highly processive motor will require less time to travel to the final destination than motors with low processivity. The release rate of the first nucleotide is dependent on the local microtubule concentration as the motor needs to diffuse and attach to the microtubule, yet the following ATP turnover rate is independent of microtubule concentration as the motor continues to walk along the microtubule [20]. However, reduced processivity can be beneficial in some situations. Velocity of microtubules or actin filaments is equal to the distance of the kinesin or myosin's powerstep divided by the time the motor protein is bound. Thus, the low duty ratio of skeletal muscle myosin, which bind to actin filaments, increases the overall speed of the actin displacement when multiple motors work as a team on the same filament. Kinesin-5 operates in a similar manner with a team of motors.

KINESIN-5

Kinesin-5 (kin-5) is also called kinesin spindle protein, KSP, or Eg5 in vertebrates and BimC is yeast. It is responsible for regulating and organizing the bipolar mitotic spindle during anaphase in eukaryotic mitosis and meiosis by sliding antiparallel microtubules apart [2] [25] [26, 27]. Kin-5 aligns the short microtubule bundles in the mitotic spindle by cross-linking and moving the plus-ends of

antiparallel microtubule [26, 28]. The shape, size, and function of the mitotic spindle depend on the motility and shape of the kinesin [25].

Kinesin-5 is a homotetramer containing two pairs of plus-end directed heads that walk along overlapping microtubules to separate the two poles during mitotic spindle formation and to pull apart the chromosomes [2, 26]. According to a phylogenic study on the kinesin superfamily by Miki et al., kin-5 is the most conserved kinesin in the superfamily, found in yeast and higher order plants in addition to animals. The structural domains, shown in Figure 4, include the neck linker downstream from the catalytic core and a BimC box close to the C-terminus with coiled-coils in between. The BimC box[1] is phosphorylated by the p34/Cdc2 kinase and localized to the microtubules [2].

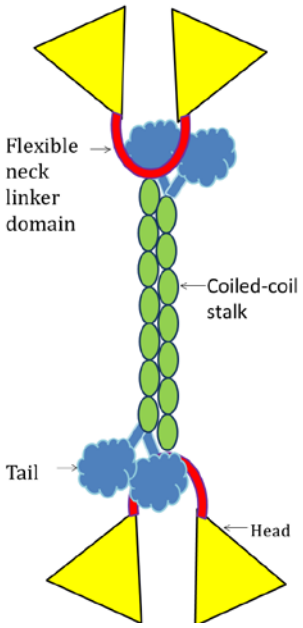

Figure 4: Structure of kinesin-5

Kinesin-5, a homotetramer, consists of 3 domains: head, coiled-coil stalk, and tail. In wild-type kin-5, the 4 heads are identical. In many assays, a DIMER was used with only one pair of plus-end directed heads. Diagram not drawn to scale.

Mitosis, the process of gene duplication and chromosome separation in cell division, uses the mitotic spindle, a subcellular protein machine consisting of dynamic microtubules and kinesin and dynein motors [29]. Chromosomes are segregated during anaphase by two processes: chromosome-to-pole motility

[1] The BimC box motif was identified in a filamentous fungus, *A.nidulans*, to cause cells to remain in mitosis when mutated [2]. Kinesin-5 was formerly known as BimC [31].

(anaphase A) and spindle elongation (anaphase B). Spindle elongation in anaphase B occurs by the sliding of anti-parallel microtubule bundles by kinesin-5[2]. At the onset of anaphase B, microtubule plus-ends are concentrated at the cell equator, which increases the overlap zone for easier cross-linking by kin-5 [29]. Figure 5 diagrams kin-5's role in chromosome segregation.

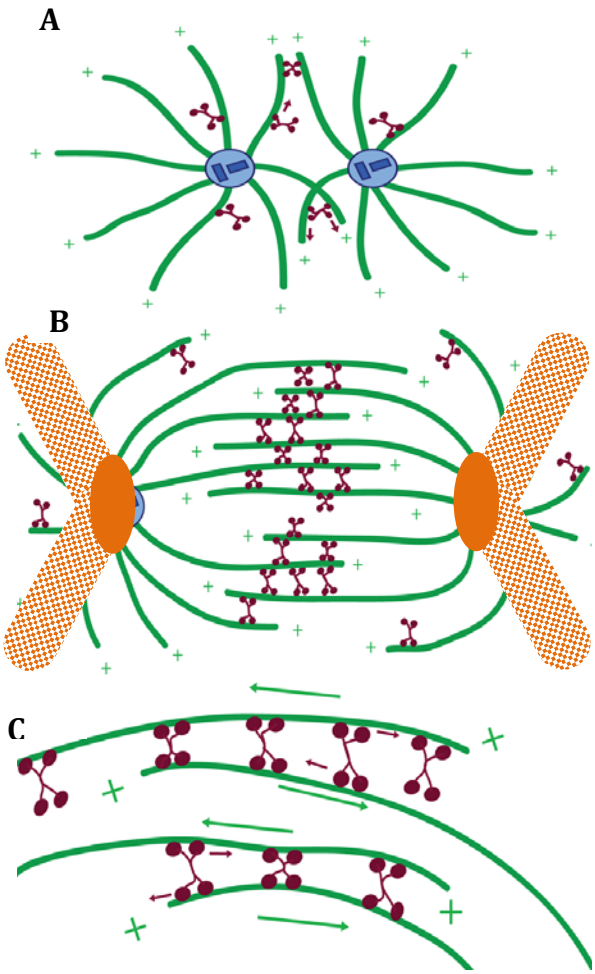

Figure 5: Kinesin-5 walking along anti-parallel microtubules

A. Kin-5 crosslinks the short microtubule bundles (green) to organize the centrosomes (blue) to form the mitotic spindle.
B. Kin-5 works in teams, making the microtubule move quickly to separate the chromosomes (orange).
C. The motors walk along two anti-parallel microtubules toward the plus-end direction of each. Figure adapted from [57].

Kin-5 walks *in vivo* at approximately 20 nm/s toward the plus-end of a microtubule. When the protein is cross-linking two microtubules, as in mitosis, this produces a relative sliding of 40 nm/s [26], comparable to the rate at which the spindle poles separate [30]. Single molecule experiments, as measured by optical traps, showed discrete steps with the average length of 8.1 ± 0.1 nm, which is consistent with the size of

[2] Exemptions to this *C. elegans* embryos, where kin-5 acts as a braking mechanism, and *S. pombe*, where a proposed kin-6 pushes the poles of the spindle apart [29].

tubulin heterodimers along a protofilament and the same size as conventional kinesin [31]. Even in saturating ATP concentrations, the maximum speed of kin-5 is markedly different than kin-1. Kin-1 can run 2.1 μm at 990 nm/s [14], whereas kin-5 has unloaded run lengths of 67±7 nm, approximately 8 steps, and an unloaded maximum velocity of 100 nm/s *in vitro* [31], which presents an order of magnitude difference between the two motors. In addition, kin-5 dissociates from microtubules before it slows or stalls when large loads are applied, contrary to kin-1.

Kin-5 is considered slow with low processivity compared to other motors in the kinesin superfamily [1, 7]. However, kin-5's processivity is difficult to accurately measure since it is a tetramer that binds to two microtubules. If the duty ratio was low for one pair of heads, then the chances of both sets of heads binding to microtubules would reduce by the square of the duty ratio [32]. Optical trap experiments in various nucleotide states measured the run lengths and determined that, although large loads could cause kin-5 to unbind from the microtubule, the direction of unbinding was independent of the applied force; this suggested the load caused a general disruption in the conformation rather load-induced dissociation [16]. The experiments also revealed that the majority of

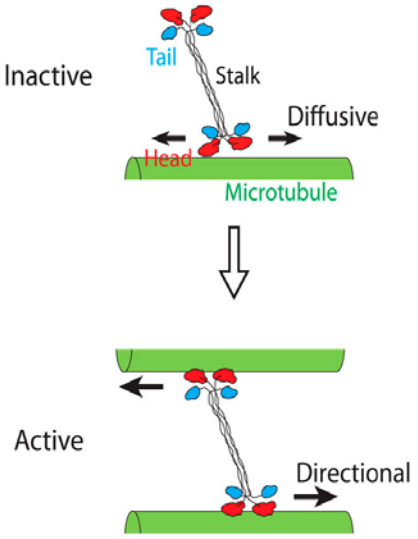

Figure 6: Kin-5 regulation

Kinesin-5 is inactive and simply diffuses along on microtubule only until both sets of heads bind to microtubules. Figure adapted from [53].

kin-5 dissociation occurred in the weakly-bound ADP state where there was "premature ADP binding" in low to moderate loads. The load independence and high tendencies of ADP dissociation verify head-to-head communication and that the chemo-mechanical cycle controls processivity instead of external loads [16].

It is hypothesized that the processivity is linked to function; many kin-5 motors are present in the overlapping chromosomes and work together as a team to maintain the mitotic spindle and slide the microtubules apart. As a team of motors, like skeletal muscle myosin, the motor proteins generate the force required to slide the chromosomes and pull the mitotic poles apart, although the individual motors only remain attached to the chromosomes for a limited number of steps [26, 12, 33].

Figure 7: Kinesin head with neck linker domain

The structure of kinesin-1 head (from rat dimer) shows the neck linker (14 amino acids long) in black. Image from [52].

The regulatory mechanism for kinesin-1 requires binding to both a microtubule and cargo before it walks along with ATP hydrolysis [20]. However, a different regulatory mechanism may be used for kin-5 as the microtubule serves as both the track and cargo [26]. As shown in Figure 6, kin-5 is able to diffuse linearly on the microtubule when only one pair of heads is bound; when the second side binds to an anti-parallel microtubule, the kinesin begins to walk processively [25]. This would make the motor more efficient in hydrolyzing ATP and

may affect its processivity by dissociating to "check" if the other end is bound. However, this regulatory mechanism has not been determined.

Neck Linker Domain in Kinesin-5

As discussed previously, the neck linker domain is responsible for force generation as the main conformational change occurs there. The length and structure of the neck linker domain differs significantly between kinesins. The first fourteen amino acids are conserved between kin-1 and kin-5, while kin-5 contains an additional four amino acids closer to the coiled-coil [34].

In kin-1 and kin-2, it was shown that processivity scales with the neck linker length and that the neck linker affects binding of ATP [35, 14]. By altering the length of the neck linker domain, it was recently verified that the length of the neck linker domains affects the processivity in unloaded kinesin motor proteins rather than altering the rate constants of ATP hydrolysis [12]. Highly processive motor proteins that transport

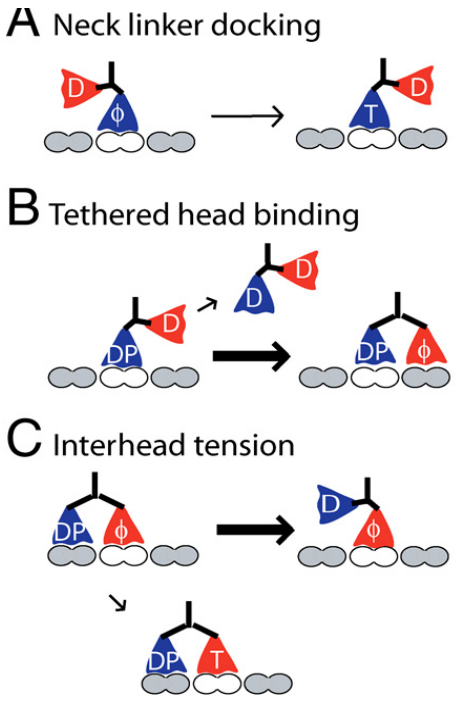

Figure 8: Roles of neck linker domain.

A. Docking to the microtubule to move the free head toward the next binding site.
B. Tethering the heads together when not bound.
C. Providing interhead tension between the heads to transmit force. Figure from [12].

cargo long distances, such as kin-1, have shorter neck linker domains [14]. Kin-5, however, is the opposite: it has a longer neck linker domain and is minimally processive [14, 33]. Previous experiments shortening the neck linker domain of kin-5 to 14 amino acid residues enhanced processivity and velocity to match kin-1. This provided the basis for the hypothesis that processivity is not due to differences in kinetics of the ATP hydrolysis cycles of the kinesin families but rather to differences in the chemomechanical pathway [12].

Although the core motor domains are structurally conserved between kin-1 and kin-5 and the motors share over 40% sequence identity, crystallographic models reveal that less of the neck linker docks in kin-5 than in kin-1. A hypothesis for this was developed by Lang et al. based on a region that changes conformation upon ATP binding called the cover-neck bundle between the N-terminal end of the motor head and the first part of the neck linker. In kin-1, this region is longer, which would be preferred in force generation [34]. As kin-5 works in teams, the force generation and docking efficiency would not be as crucial as in kin-1.

The interhead tension that develops when both heads are bound to microtubules has been estimated by molecular dynamics simulations as 15-35 pN for kin-1 [6]. Since the tension occurs primarily in the neck linker domain [36, 12, 5], a longer neck linker would make it more compliant and potentially reduce the tension that occurs when both heads are bound to microtubules. A change in tension would require compensation if the same force was required for gating in

kin-5 as in kin-1 or kin-5 would need to follow different gating and/or chemo-mechanical pathways.

ANTI-CANCER

Chemotherapy for antimitotic approaches to cancer generally target tubulin. *Vinca* alkaloids are used to treat leukemia and Hodgkin's lymphoma, and paclitaxel (Taxol) is approved for metastatic breast and ovarian carcinomas. These drugs interfere with the assembly or disassembly of microtubules, which causes mitotic arrest and eventual cell death [29, 37]. However, cells exposed to prolonged treatment can develop resistance to the drugs and the drugs have intense side effects [29]. The major side effect is neurotoxicity since microtubules are involved with mitosis-dependent cytoskeletal and nervous functions. Inhibiting microtubule dynamics causes dendritic spines in the central nervous system to modulate shape via regulation of the actin skeleton. Several mental retardation syndromes have been linked to altered dendritic spine morphology [29, 38]. To mitigate the problems associated with mitosis-dependent tubulin, other strategies involving microtubule- and mitotic-associated proteins are being investigated. As proper formation and organization of a bipolar spindle is

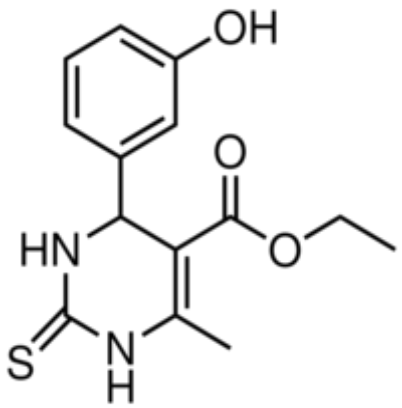

Figure 9: Chemical structure of monastrol

Monastrol inhibits kin-5 by inducing structural changes. Without the functioning motor protein, cancer cells are arrested in anaphase and prevented from dividing. Figure taken from reference [40].

required in cell division, and therefore present in proliferating cancer cells, inhibition of kin-5 is a potential approach for developing cancer treatments that block cell division [39, 37, 27].

Inhibition of kin-5 leads to cell-cycle arrest during mitosis with cells exhibiting a monopolar spindle, called a monoester, instead of two mitotic poles [27]. Monastrol (*4-(3-Hydroxyphenyl)-6-methyl-2-thioxo-1,2,3,4-tetrahydro-4H-pyrimidin-5-carboxylic Acid Ethyl Ester*) was the first small molecular inhibitor of kin-5 (See Figure 9 for chemical structure) [27, 40, 37]. This inhibitor triggers structural changes throughout the motor domain. Studies have shown that monastrol does not exhibit neurotoxicity or other negative effects in dendritic function [27].

As kin-5 is a current target for antimitotic drugs, a better understanding of its mechanism should aid the future development of drugs for cancer treatment by inhibition of this motor.

ENGINEERED MOTOR PROTEINS

The ability to engineer neck linker domains of varying lengths or with heads of other different kinesins permits the creation of novel kinesin chimaeras. These engineered motors provide models to better study the mechanism and kinetics of kin-5, specifically in regard to the neck linker domain.

In addition, while the functioning motor protein is a homotetramer, much can be understood by testing the motility and various kinetic rates of

heterotetramers, dimers, and monomers. For many kinetics assays, the dimer must be used to obtain the desired rate for one pair of heads. Since the coiled-coils of the tetramer are entangled, terminating too close to the motor may lead to unintended consequences in the kinetic rates. The coiled-coil and/or tail may be involved with head regulation, so a stable and well-characterized coiled-coil with proper dimerization can be substituted when constructing dimers.

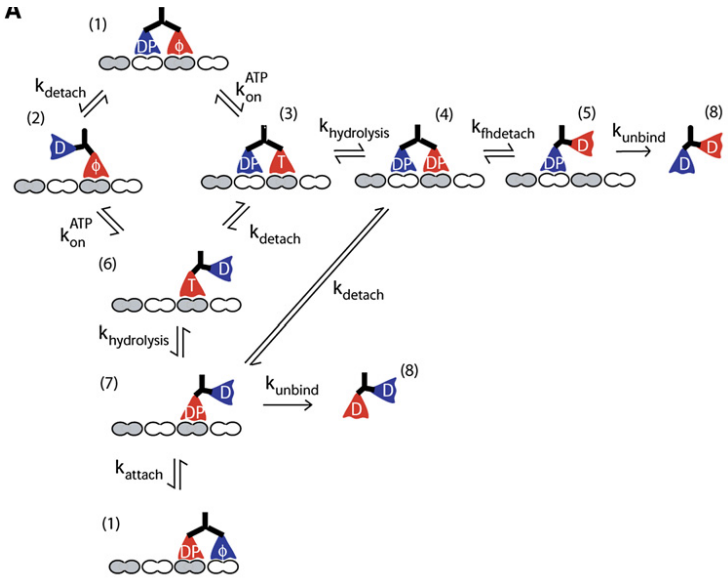

Figure 10: 8-state chemomechanical cycle of kin-1

This cycle and the cycle in Figure 3 were used as the basis for the computational experiments. Image from [37].

PROJECT HYPOTHESIS

Alternatives to the "consensus" chemo-mechanical pathway were developed to test for alternative possibilities that may explain how changing the neck linker length significantly changed kin-5's processivity and velocity. We hypothesized that interhead tension on the neck linker instigates alternate strain-dependent pathways and that tethered-head attachment can occur before hydrolysis in some instances. We aimed to test this hypothesis by creating computational simulations that included strain calculations and by performing kinetics assays that tested different

dissociation possibilities, which could strengthen the argument for or against a novel or tension-dependent chemo-mechanical pathway.

The computational model used was based off of that used by Muthkrishnan et al., shown in Figure 10. I performed all of the modifications to the MATLAB code and analyzed the simulation results. The pelleting assays were completed with much assistance from David Arginteanu. I analyzed the results. The fluorescence dissociation assay was performed by Yalei Chen. I analyzed the STP movies. I also worked on the molecular biology of creating the mutant human kin-5 construct.

Chapter 2

Literature Analysis of Rate Constants

The conventional chemo-mechanical stepping cycle with corresponding rate constants, illustrated in Figure 3, shows how kinesin-1 uses two heads to walk along the microtubule. However, it was merely assumed that kin-5 follows the same cycle with only one additional transition step to allow for docking of the neck linker domain. Since the run length and velocity of this kinesin vary so greatly from conventional kinesin (1/12 run length and 1/8 velocity compared to kin-1) [12], it is conceivable that it adheres to a different chemo-mechanical cycle. To determine how the cycle would vary, a thorough literature analysis was conducted. While kin-1 has been intensively studied, there are far fewer labs actively publishing data on kin-5 with the labs of Steven Rosenfeld at Columbia University and Susan Gilbert at the University of Pittsburgh providing most of the published kinetic data.

Rate Constants from Rosenfeld and Gilbert Labs

The Rosenfeld lab performed experiments using spectroscopic probes for fluorescence resonance energy transfer (FRET) to obtain a model with matching rate constants. Methods for obtaining the kinetic parameters include five different FRET donor acceptor combinations, fluorescence enhancement of MDCC-labeled phosphate-binding protein, and turbidity in a stopped flow spectrometer at 350 nm [33, 41]. Rosenfeld proposed a hybrid-like model for stepping that involves an ATP binding-dependent docking of the neck linker and a rolling of the head during ATP

hydrolysis where the head is weakly bound. The additional rolling is hypothesized to generate enough flexibility for the diffusive search for the next binding site while remaining rigid in other states [33]. A mutant of Cysteine-light Eg5-367 was used with several neck linker probes to enable FRET [33]. These mutant constructs may have affected the rigidity of the neck linker, and they are monomers, which only consider the actions of one head without dimerization. Thus, some rate constants, such as rear-head detachment or tethered-head attachment, may not accurately reflect the communication between the two head with the neck-linker.

The Gilbert lab obtained their kinetics values from Eg5-513 constructs, which is a dimer rather than a monomer. They used fluorescence and pulse chase experiments for ATP binding, stopped flow techniques for rear-head detachment and ADP release, and turbidity assays for attachment rates. They accepted ATP hydrolysis as the rate-limiting step after eliminating three other possibilities to explain their result of no burst of product formation in pulse-chase and stopped-flow assays [42]. While their logic for determining the rate-limiting step appears reasonable, they had another rate constant, rear-head detachment, that was slower than or equal to the rate of ATP hydrolysis. Interestingly, the steady-state parameters, measured by ATPase experiments, were slow with a k_{cat} of approximately 0.5 s^{-1}. With the step size is 8 nm, the resulting velocity would be only 4 nm/s. The authors notice this was "lower than would be predicted based on the motility assays" and explained that the value includes microtubule detachment and rebinding, which are diffusion dependent [43]. A length of the coiled-coil was

chosen where dimerization occurred but not tetramerization. It is possible that the length was too short to stably hold the heads together as insufficient dimerization would explain the slow ATPase values and may blur the rate-limiting step data.

Table 1: Rate constants in literature

Rate Constant	Gilbert Lab [a]	Rosenfeld [b,c]
k_rear_detach	6.6 ± 0.1 s^{-1}	8.7 ± 13.9 s^{-1}, [c]
k_ATP_on	1.2 ± 0.1 $uM^{-1}s^{-1}$	1.1 ± 0.1 $uM^{-1}s^{-1}$
k'_ATP_on	1.4 ± 0.6 s^{-1}	7.9 ± 0.9 s^{-1} [c]
k_neck_linker	---	62 ± 17 s^{-1}
k_hydrolysis	5 – 10 s^{-1}	10.3 ± 0.3 s^{-1}
k_attach	Not valid in stochastic simulations	
k'_attach	9.7 ± 1 s^{-1}	44.1 ± 6.5 s^{-1}, [c]
k_ADP_off	28.2 ± 0.5 s^{-1}	76 ± 15 s^{-1}
k'_ADP_off	---	0.3 ± 0.1 $uM^{-1}s^{-1}$
k_off	9.7 ± 1 s^{-1}	8.6 ± 0.1 s^{-1}, [c]

[a] Data are from Krzysiak and Gilbert [42].
[b] Data are from Rosenfeld et al. [33].
[c] Data are from Behnke-Parks et al. [41].

Chapter 3

Computational Modeling

Methods - Stochastic Simulations

The computational approach is based off of the simulation used by Muthukrishnan et al. [36] and similar to that used by Shastry and Hancock [14].

A Monte Carlo method using the Gillespie Stochastic Simulation Algorithm [44],

$$t = \frac{1}{k} ln \frac{1}{rand\#}$$

was used with discrete states corresponding to different nucleotide states in the kinesin hydrolysis cycle. The fastest transition time, *t*, was chosen as the minimum possible dwell time independent of the direction of the previous transition.

The motors began in State 1 with two heads bound, one with no nucleotide and other with ADP+P_i. Individual motors continued throughout the cycle until they detach. A step was counted each time the motor returns to State 1. The mean and standard deviation of the run length and velocity of 10,000 individual motors was recorded.

Methods - Force-Dependent Rates

To account for the change in run length and velocity with a different neck linker domain, the neck linker was modeled as a worm-like chain (WLC). The force required to extend a chain a distance *x* is calculated as:

$$F_{WLC}(x) = \frac{k_B T}{L_p}\left[\frac{1}{4}(1-\frac{x}{L_c})^2 - \frac{1}{4} + \frac{x}{L_c}\right]$$

where k_B is the Boltzman constant, T is the absolute temperature, L_p is the persistence length, L_c is the contour length of the polymeric chain, and x is the end-to-end distance. The values used, based on previous molecular dynamics simulations, were an L_p of 0.7 nm and L_c of 0.364 nm per amino acid [45]. The end-too-end length was 4 nm, which is approximately half the step length and, therefore, neither a conservative nor liberal estimate of the neck linker docking. The force depends greatly on the contour length, which is proportional to neck linker length. Although it was shown that the WLC model may be inaccurate, the theory of the polymeric model fits better than the constant stiffness or reflecting models, as described by Kutys et al [45].

Some rate constants were modeled as force-dependent using the Bell Equation [47, 48],

$$k_{force-dependent} = k_0 * e^{\frac{F*b}{k_B T}}$$

where F is the force calculated from WLC and b is the characteristics bond length, 0.5 nm. The constants affected were rear-head detachment, attachment, and ATP binding with rear-head gating.

METHODS - USER-CONTROLLED ROUTES

In efforts to make the model more controllable, there were several options for switching pathways on or off listed at the top of the main MATLAB script. The

user was able to choose whether rates were strain dependent or not and if the gating and hydrolysis bifurcations were both permitted or whether one route was blocked. In a similar manner, the rate constants for the two hydrolysis pathways could be either the same or different. Any of these options could be changed by simply entering a 'y' or 'n' for each option before running the script. If both routes were marked 'y,' then the simulation considered both options using the Gillespie Algorithm without any other bias.

LITERATURE PATHWAYS

Although verifying all of the individual rate constants was outside of the scope of this project, the suggested pathway from each lab was analyzed and compared against each other and against the measured rates of other kinesins, primarily kin-1. A model of the consensus stepping cycle was created in MATLAB (See Figure 11), and rate constants from literature were used to analyze the run length and velocity. The model was verified using data for rate constants, run length, and velocities of kin-1 (data not shown).

Three primary simulations were performed: one using data from Gilbert's lab experiments on dimeric motors, one using data from Rosenfeld's lab gathered using mostly FRET techniques, and one using a combination, biased to increase the velocity. The rates that were included in the model replicating their proposed pathway are provided in Table 1.

The tethered head attachment rate is dependent on the local concentration of tubulin and expressed as second-order rates in literature; however, since the motor is already attached via the tethered head, the tubulin concentration can be considered constant, and the transition can be modeled as a first-order rate. Tethered head attachment (k_{attach}) was altered to force a run length of approximately 64 nm, or 8 steps.

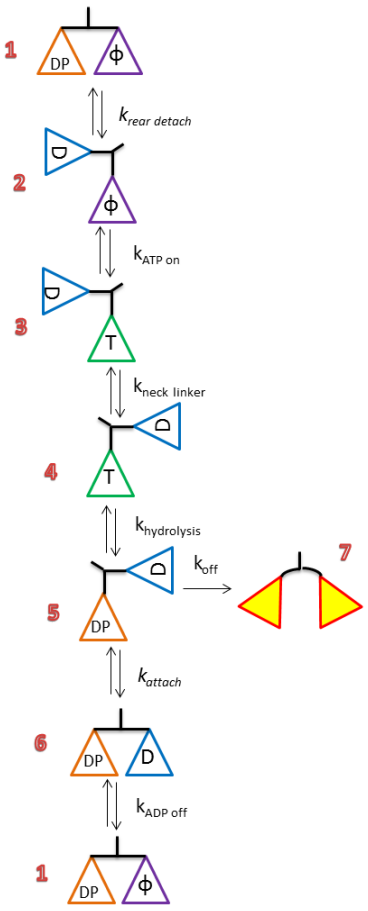

Figure 11: Literature chemo-mechanical cycle of kin-5

This "consensus" pathway was used to model the rate constants provided in literature by the labs of Gilbert and Rosenfeld. State 4, following the change in neck linker orientation, was only included when a rate was provided.

The simulation inputs and outputs modeling Gilbert, Rosenfeld, and the combination pathways can be found in Table 2-Table 7. The resulting run lengths and velocities represent the average value of 10,000 individual motors; three results are shown to demonstrate the slight variations in the stochastic model. The standard deviation is larger than the mean (See Table 7), which is expected for stochastic simulations. Using the Gillespie algorithm produces a reliable overall exponential distribution when many samples are used[47]. A larger sample number (number of motors in this case) will produce more accurate results (similar means) that will not affect the reported standard deviation of each simulation.

The velocity from the models was consistently significantly slower than observed, with maximum velocities of 20 nm/s for Gilbert's values and 30 nm/s for Rosenfeld's values. Even the model that was biased for a larger velocity with rate constants from many sources had a velocity of 35 nm/s. While this value is similar to the 40 nm/s that the motor protein travels *in vivo*, it is much slower than the expected 100 nm/s for unloaded speeds at saturating ATP conditions [31]. The slow velocities could be due to the presence of two rate-limiting steps: ATP hydrolysis and rear-head detachment. With one rate as low as 10 s^{-1}, the maximum rate would be 80 nm/s, and with two slow rates, the maximum rate is decreased in half to 40 nm/s. The rear-head detachment rate was altered to be slightly larger than the hydrolysis rate to establish a single rate-limiting step and provide a better comparison between the models.

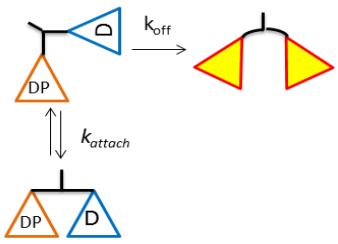

Figure 12: Possibility of detachment

When the motor protein is attached to the microtubule in the weakly-bound ADP-P_i state, the motor could either dissociate (k_{off}) or continue in the stepping cycle by attaching the tethered head (k_{attach}).

The tethered-head attachment rates required for a run length of eight steps were lower using Gilbert's data than Rosenfeld's or a combination when the same dissociation rate from the ADP state was used. This is interesting since the probability of detaching per step can be calculated by

$$Probability\ of\ detachment = \frac{k_{off}}{k_{off} + k_{attach}}$$

To achieve the observed run length, the probability of detaching per step is 11% in the Gilbert model and 5-8% in the Rosenfeld model. This difference makes Gilbert's

model appear appears less processive, however some reverse rates (most notable states 1 to 6) are not provided in the papers, so the motor appears to have a lower overall chance of returning to the possible state of detachment. This makes comparing the models from the two labs more difficult.

Table 2: Inputs and results of Gilbert lab minimum hydrolysis value

This simulation used the minimum rate for hydrolysis (6 s^{-1}) all other mean rate constants reported by Gilbert [42, 43]. The tethered-head attachment rate (*k_attach*, shown in italics) was adjusted to achieve a mean run length of 64 nm.

Rate Constant	Value (s-1 unless otherwise labeled)
k_rear_detach	6.6
k_ATP_on	1.2 * ATP $s^{-1}uM^{-1}$
k'_ATP_on	1.4
k_hydrolysis	6
k'_attach	9.7
k_ADP_off	28.2
k_off	9
k_attach	*75*

Run Length (nm)	Velocity (nm/s)
65.4	17.1
65.8	17.3
67.0	17.1
Mean: 66.1	**Mean: 17.2**

Table 3: Inputs and results of Gilbert lab maximum hydrolysis value

This simulation used the maximum hydrolysis rate (10 s^{-1}) reported by Gilbert [42, 43] and an arbitrarily-increased **rear-head detachment rate** (k_rear_detach) of 12 s^{-1} so that hydrolysis could remain as the rate limiting step.

Rate Constant	Value (s-1 unless otherwise labeled)
k_rear_detach	12
k_ATP_on	1.2 * ATP $s^{-1}uM^{-1}$
k'_ATP_on	1.4
k_hydrolysis	10
k'_attach	9.7
k_ADP_off	28.2
k_off	9
k_attach	*75*

Run Length (nm)	Velocity (nm/s)
63	21
65	21
68	21
Mean: 66	**Mean: 21**

Table 4: Inputs and results of Rosenfeld lab values

This simulation used the mean rate constants reported by Rosenfeld [41, 33]. The **tethered-head attachment rate** (k_attach, shown in italics) was adjusted to 165 $^{s-1}$ to achieve a mean run length of approximately 64 nm.

Rate Constant	Value (s-1 unless otherwise labeled)
k_rear_detach	8.7
k_ATP_on	1.1 * ATP $s^{-1}uM^{-1}$
k'_ATP_on	19
k_neck_linker	62
k_hydrolysis	10.3
k'_attach	44.1
k_ADP_off	76
k_off	9
k_attach	*165*

Run Length (nm)	Velocity (nm/s)
65	29
65	29
64	29
Mean: 65	**Mean: 29**

Table 5: Inputs and results of Rosenfeld lab values limited by hydrolysis

This simulation used the mean rate constants reported by Rosenfeld [41, 33] with the exception of the rear-head detachment rate, which was increased to 12 s^{-1} so that hydrolysis was the rate limiting step. This modification was done to compare the results using values from Gilbert's lab.

Rate Constant	Value (s-1 unless otherwise labeled)
k_rear_detach	12
k_ATP_on	1.1 * ATP $s^{-1}uM^{-1}$
k'_ATP_on	19
k_neck_linker	62
k_hydrolysis	10.3
k'_attach	44.1
k_ADP_off	76
k_off	9
k_attach	*165*

Run Length (nm)	Velocity (nm/s)
64	31
62	31
63	31
Mean: 63	**Mean: 31**

Table 6: Basic rate constants from multiple sources in combination simulation

This simulation used available rate constants from kin-5 experimental data and additional rates from kin-1. This model, like the above Gilbert and Rosenfeld models, did not take neck linker length into account.

States	Rate Constant	Value	Source
1 -> 2	k_rear_detach	12 s^{-1}	[42]
2 -> 1	k'_rear_detach	0.1 s^{-1}	[36]
2 -> 3	k_ATP_on	1.2 $uM^{-1}s^{-1}$	[33, 42]
3 -> 2	k'_ATP_on	2 s^{-1}	[42]
3 -> 4	k_neck_linker	60 s^{-1}	[33]
4 -> 5	k_hydrolysis	10 s^{-1}	[33, 42]
5 -> 4	k'_hydrolysis	0.1 s^{-1}	[19]
5 -> 6	*k_attach*	*100 s^{-1}*	
5 -> 7	k_off	9 s^{-1}	[41, 42]
6 -> 5	k'_attach	40 s^{-1}	[41]
6 -> 1	k_ADP_off	70 s^{-1}	[33]
1 -> 6	k'_ADP_off	0.3 $uM^{-1}s^{-1}$	[33]

Table 7: Results from simulations of rate combinations model

Run Length (nm)	Std. Dev. (nm)
66	69
66	70
66	71
Mean: 66	

Velocity (nm/s)	Std. Dev. (nm/s)
34	16
34	16
34	17
Mean: 33.8	

INVESTIGATIONAL MODEL DESCRIPTION

Stochastic simulations of the kinesin chemomechanical cycle were performed in MATLAB to assess whether the changes in run length and velocity of kin-5 are caused by a different chemomechanical cycle than previously believed. The previous assumption is that ATP hydrolysis of the bound head precedes the attachment of the tethered head to the microtubule (State 4 to 5 in Figure 13). This is a reasonable

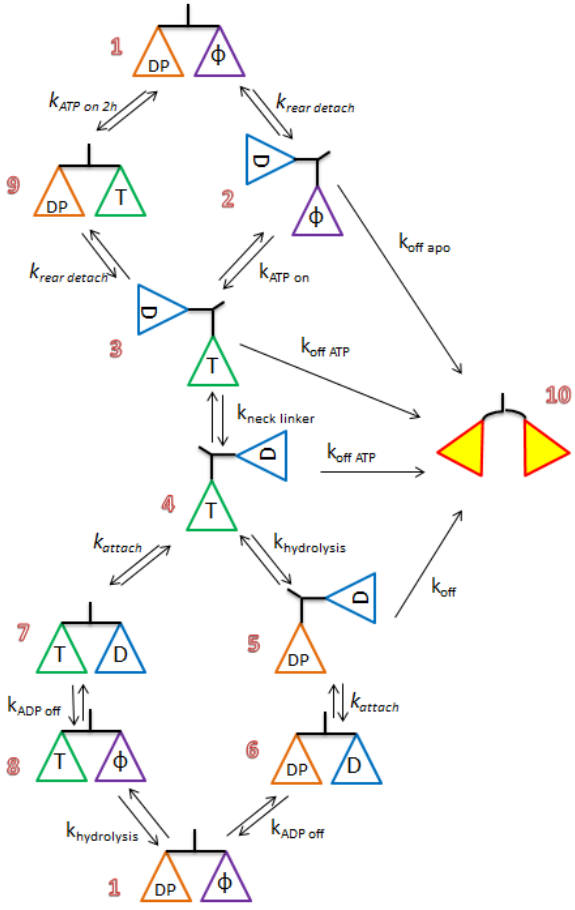

Figure 13: Investigational chemo-mechanical pathway with two bifurcations

This chemo-mechanical model includes gating (States 2 and 9) and a novel hydrolysis pathway (States 7 and 8). Multiple possibilities of dissociation were added to account for the low processivity.

assumption for kin-1 since the rate of hydrolysis is fast. Kin-5 has a slow, potentially rate-limiting rate of hydrolysis; hence, the assumption is not as sound. It is possible that the tethered head attaches to the microtubule and its ADP dissociates to form a strong binding state before hydrolysis occurs (State 4 to 7 in Figure 13). The chemomechanical cycle could be non-exclusive, dependent on internal stress, or proceed exclusively through one pathway.

The initial, investigational MATLAB simulation stemmed from the combination pathway shown in Figure 10. The novel cycle, illustrated in Figure 13, included both front- and rear-head gating pathways that depend on internal strain and a novel bifurcation for an alternate hydrolysis pathway.

The first possible alternate pathway is linked to gating, similar to the pathway for kin-1, shown in Figure 3. The non-exclusive mechanisms of front- and rear-head gating are linked to internal tension in the neck linker

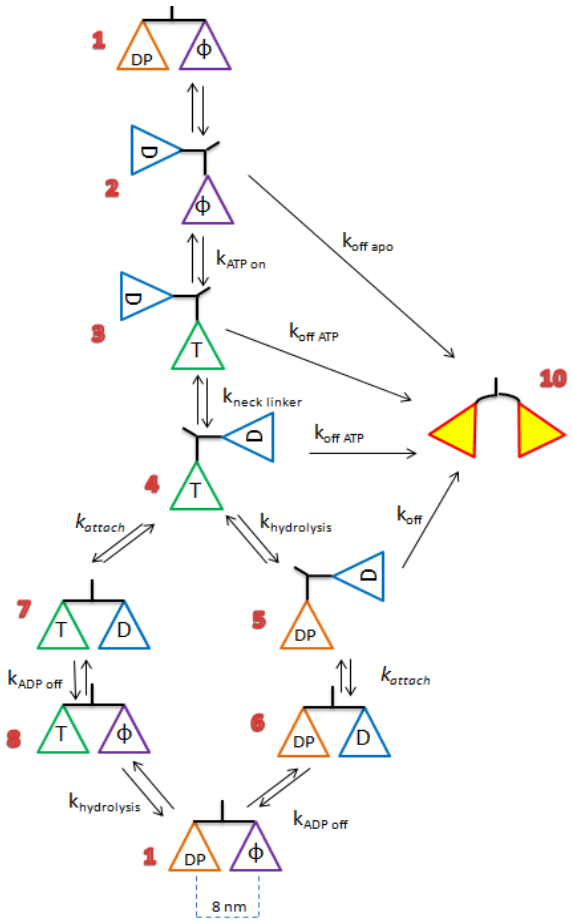

Figure 14: Investigational chemo-mechanical pathway with one bifurcation

This chemo-mechanical model includes a novel hydrolysis pathway (States 7 and 8). Multiple possibilities of dissociation were added to account for the low processivity. In one cycle, one head moves 8 nm.

domain [36]. Although the literature pathways for kinesin-5 follow front-head gating only [42, 43, 41, 47, 33], the possibility of both pathways may help explain the phenomenon associated with changing the neck linker domain length. For simplification, this bifurcation was eliminated when considering the effects of the alternate hydrolysis pathway with the resulting pathway as shown in Figure 14.

The alternate hydrolysis pathway eliminates the step with the primary method of microtubule dissociation, and if the “literature pathway”, where hydrolysis precedes tethered-head attachment, is eliminated completely, then the kinesin always has one or two heads that are strongly bound to the microtubule. While the apo and ATP states and strongly bound in kin-1, it is possible that either the apo or ATP-bound state in kin-5 may be weakly bound; this could explain the reduction in processivity. With this mindset, three new possibilities for detachment from the microtubule were added: one where the motor protein can dissociate when one apo head is bound (from State 2) and two where only head with ATP is attached (States 3 and 4). Minimum rates of dissociation for the ATP-bound and apo states were calculated, keeping detachment in the ADP-bound state constant.

The neck linker was modeled as a worm-like chain with the rear-head detachment rate and the tethered-head attachment rate strain-dependent. In most cases, the attachment rate was altered to force a run length of 8 steps, as discussed with the literature pathway. In other instances, however, the tethered-head attachment rate was an order of magnitude higher than the "competing" rates to bias the route toward the desired direction without eliminating the other route as a

possibility. The attachment rate was particularly important as the ratio between the ADP dissociation rate (k_{off}) and the attachment rate (k_{attach}) determines the rate at which the motor protein dissociates from the microtubule. With the hydrolysis bifurcation, the rate of that the tethered head attaches to the microtubule was also crucial in determining which pathway the motor protein. The probability of the motor following the alternate hydrolysis pathway is given by the equation

$$Chance\ of\ alternate\ hydrolysis\ pathway = \frac{k_{attach}}{k_{attach} + k_{hydrolysis}}$$

Since Gilbert's lab used a dimer and Rosenfeld's lab used a monomer, some rates varied substantially. Values, particularly reverse attachment (k'_{attach}) and ADP dissociation (k_{ADP_off}) from the monomer studies were applied to the literature pathway, where one head is bound. The rates for the same transitions from the dimer were applied to the alternate pathway where both heads remain attached. The different rates were only used in simulations where strain was not considered, and it is not expected that the different rate constants make a significant difference in the velocity or run length.

STRAIN-DEPENDENT MODEL RESULTS

The model was analyzed first with the strain-dependent literature pathway. The force, calculated by modeling the neck linker as a worm-like chain, increases as the neck linker length decreases as the contour length is dependent on the number of amino acids. As illustrated in Figure 15, the rate of rear-head detachment follows the same trend as the force required to extend the link linker, as calculated from the worm-like chain equation, since a higher interhead strain would cause the head to detach more rapidly. The tethered-head attachment rate follows the opposite trend; as the interhead strain increases, the attachment decreases since the molecule would not diffuse into a state of high strain as rapidly.

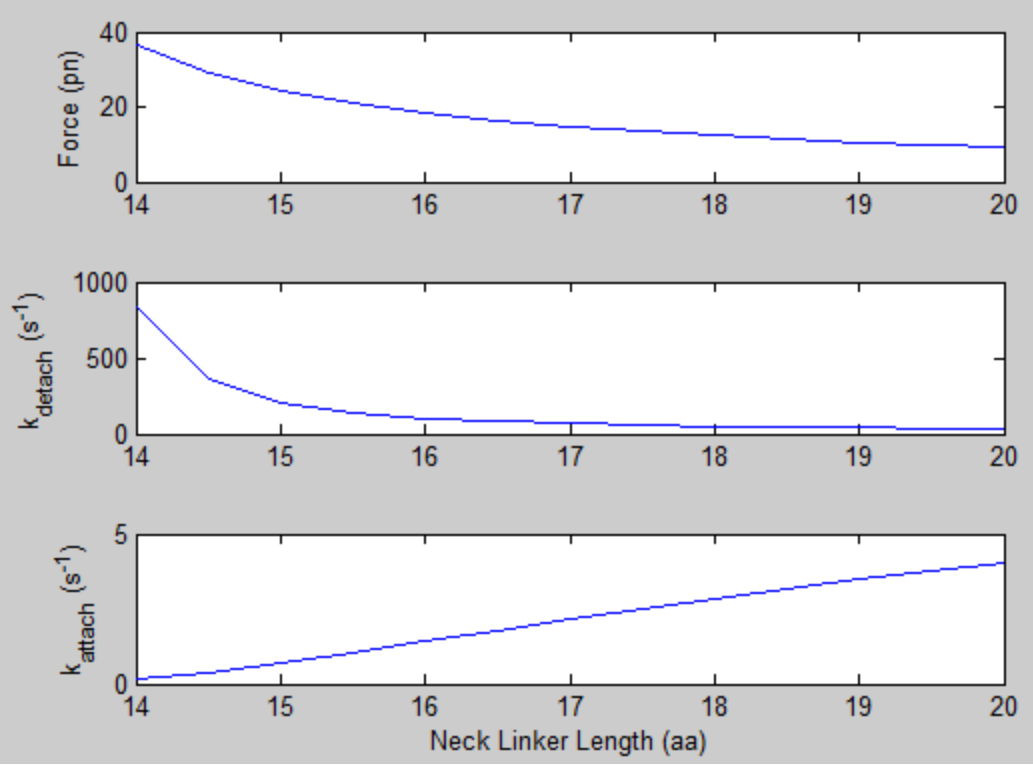

Figure 15: Worm-like chain force and rate constants

When the neck linker is modeled as a worm-like chain, the resulting force increases as neck linker length decreases. The rate constants for rear-head detachment and tethered-head attachment (both initially 12) vary to limit the time spent in the high-strained, bound state.

When strain-dependent rates were included in the consensus model, a shorter neck linker produced shorter run lengths, as seen in Figure 17. This is opposite from the experimentally observed results [12]. The attachment rate is particularly important in processivity. Decreasing the attachment rate, which occurs due to the strain from a shorter neck linker, increases the chance of dissociation, thereby decreasing the run length. Since this result does not reflect the experiments, further models did not include strain-dependent rates.

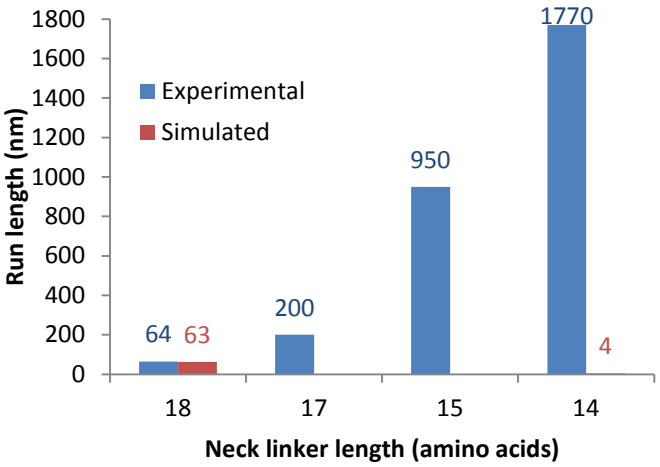

Figure 17: processivity with strain

When the rear-head detachment and tethered-head attachment rates are strain-dependent, the simulated run lengths decrease with shorter neck linker lengths while the experimental run lengths increase.

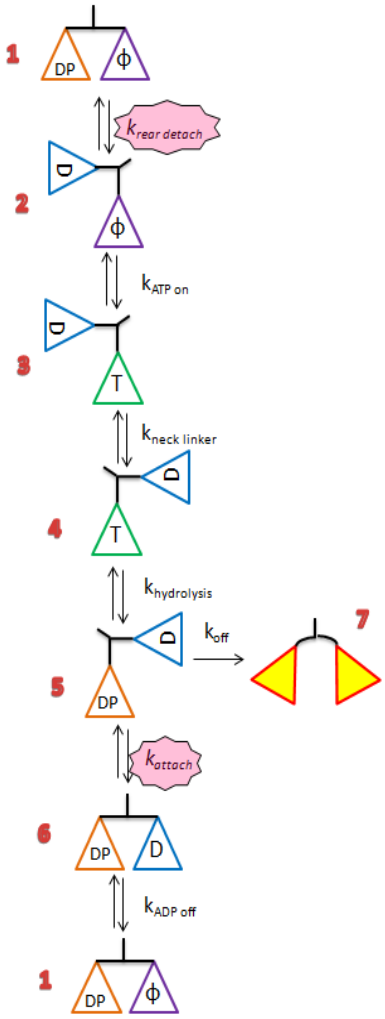

Figure 16: Chemomechanical cycle highlighting strain-dependent rates

The neck linker was modeled as a worm-like chain, and, by the Bell equation, the rear-head detachment and tethered-head attachment rates (highlighted) were modified to be strain-dependent.

STRAIN-INDEPENDENT MODEL RESULTS

Since modeling the neck linker as a worm-like chain produced simulated run lengths that were opposite from the experimental results, the strain-dependence was removed from the following simulations. The rate constants used for each scenario are provided in Table 8. There are two different values for the reverse attachment (k'_attach) and ADP dissociation (k_ADP_off) rates from measurements from kin-5 monomer or dimer.

Table 8: Rate constants used in simulations for investigational pathways

"States" refers to the transitions in Figure 14. The possible states depend on the route chosen by the user. The "d" refers to measurements from the dimer, and the "m" refers to values from the monomer. The attachment rate and off rates were varied either to force the desired run length or to bias the pathway.

States	Rate Constant	Value	Source
1 ⟶ 2	k_detach	10 s^{-1}	Near [43, 33]
2 ⟶ 1	k'_detach	0.1 s^{-1}	[37]
2 ⟶ 3	k_ATP_on	1.2 * ATP $s^{-1}\mu M^{-1}$	[43, 33]
3 ⟶ 2	k'_ATP_on	2 s^{-1}	[43]
3 ⟶ 4	k_necklinker	62 s^{-1}	[33]
4 ⟶ 5, 8 ⟶ 1	k_hydrolysis	10 s^{-1}	[43, 33]
5 ⟶ 4, 1 ⟶ 8	k'_hydrolysis	0.01 s^{-1}	[19]
6 ⟶ 5	k'_attach_m	44 s^{-1}	[33]
7 ⟶ 4	k'_attach_d	10 s^{-1}	[42]
6 ⟶ 1	k_ADP_off_m	76 s^{-1}	[33]
7 ⟶ 8	k_ADP_off_d	28 s^{-1}	[43]
1 ⟶ 6	k'_ADP_off	0.3 * ADP $s^{-1}\mu M^{-1}$	[33]
5 ⟶ 10	k_off	9 s^{-1}	[42, 43]
2 ⟶ 10	k_off_apo	0.013 s^{-1}	Experimental[3]
3 ⟶ 10, 4 ⟶ 10	k_off_ATP	0.0003 s^{-1}	Experimental[3]
5 ⟶ 6, 4 ⟶ 7	k_attach	Varies	---

[3] The results shown for the simulations used values from experiments discussed in detail in Chapter 4.

Using the values listed in Table 8 for the literature pathway only (pathway in Figure 11), the attachment rate necessary to obtain a run length of 8 steps is 100 s^{-1}, the same value for the combination pathway (See Table 6). Also, the velocity is 33 nm/s, which is closer to the combination pathway and slightly higher than the velocity from rates from either lab separately.

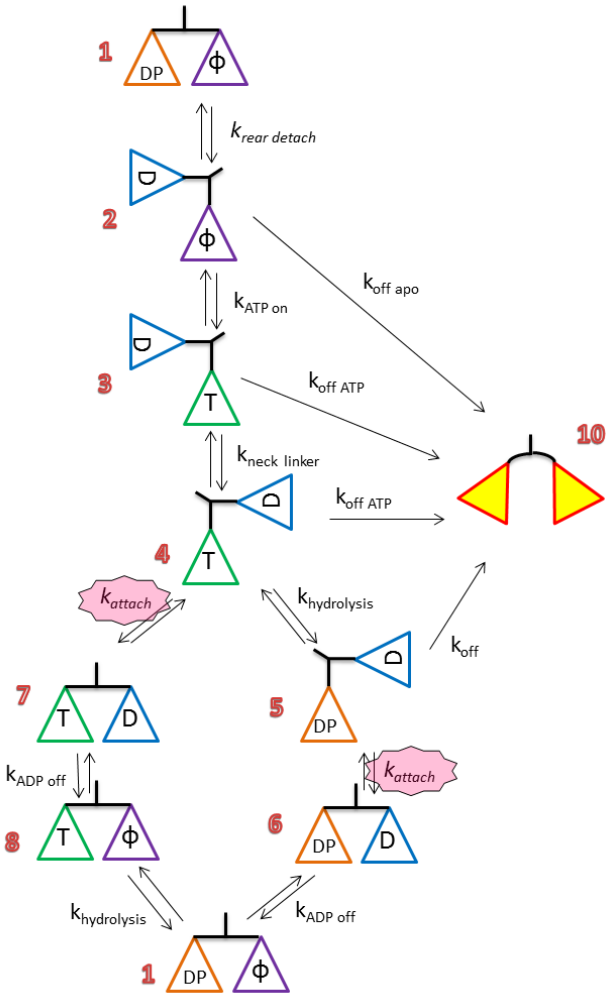

Figure 18: Chemomechanical pathway highlighting tethered-head attachment

When both pathways involving hydrolysis are possibilities, the tethered-head attachment rate (highlighted) balances between biasing the motors to take the alternate route (State 4 vs. State 7) and dissociating (State 6 vs. State 10).

When both the literature pathway and alternate hydrolysis pathway are possibilities, the necessary tethered-head attachment rate to achieve a mean run length of 64 nm is 30 s^{-1}. Figure 18 shows how the location of the attachment rate plays a major role in the pathway. The rate balances between the motors taking the alternate route and the chance of dissociation. With an attachment rate of 30 s^{-1} and a hydrolysis rate of 10 s^{-1}, the motors are three times more likely to take the alternate pathway than the literature pathway. Dissociation from the ADP-

bound state is close to hydrolysis at 9 s^{-1}.

The dissociation constants were analyzed next. If kin-5 follows the alternate hydrolysis pathway, then it would need a different method of dissociation. The simulation was run with the attachment rate at 1000 s^{-1}, so there was approximately a 1/100 chance of the motor taking the literature hydrolysis pathway. Ma and Taylor measured a rate of 110 s^{-1} using mantADP for the combination of ATP binding, ATP hydrolysis, tethered-head attachment, and ADP release [50]. The minimum rate of attachment for kin-5 would be significantly larger than 110 s^{-1} since the other rates are smaller, so a value of 1000 s^{-1} is sufficiently large. The mean run length from three trials, one with 10,000 motors and two with 1,000 motors, was about 5.9 μm. This would make kin-5 even more processive than wild-type kin-1. The velocity increased slightly to 38.9 nm, which is nearing the maximum velocity with the two limiting rates.

The model included dissociation rates for each one-head bound state, listed in Table 8 and illustrated in Figure 19. The motor protein will not dissociate from a two-head bound state [50]. It is assumed that kin-1 and kin-5 share the same strongly and weakly bound states, meaning that the motor with no nucleotide or with ATP bound is always strongly bound to the microtubule. However, there is a possibility that kin-5 is actually weakly bound to the microtubule in the apo or ATP-bound state. To test this, the minimum dissociation rates for the ATP-bound and apo states were determined in the model by biasing or forcing the motor to take the

alternate hydrolysis pathway and altering the dissociation rate to achieve a run length of 8 steps.

When the attachment rate was set at 1000 s^{-1} and the ATP dissociation rate remained at the experimental value, the apo dissociation rate from state 2 was 185 s^{-1} to force a mean run length of 64 nm. When the literature pathway was not an option and the motors never had the possibility of dissociating from the ADP-bound state, the apo dissociation rate was decreased to 140 s^{-1} to obtain the same mean run length. The ATP-bound dissociation rate from states 3 and 4 was 9 s^{-1} with the attachment rate at 1000 s^{-1} and 7 s^{-1} when the literature pathway was not an option.

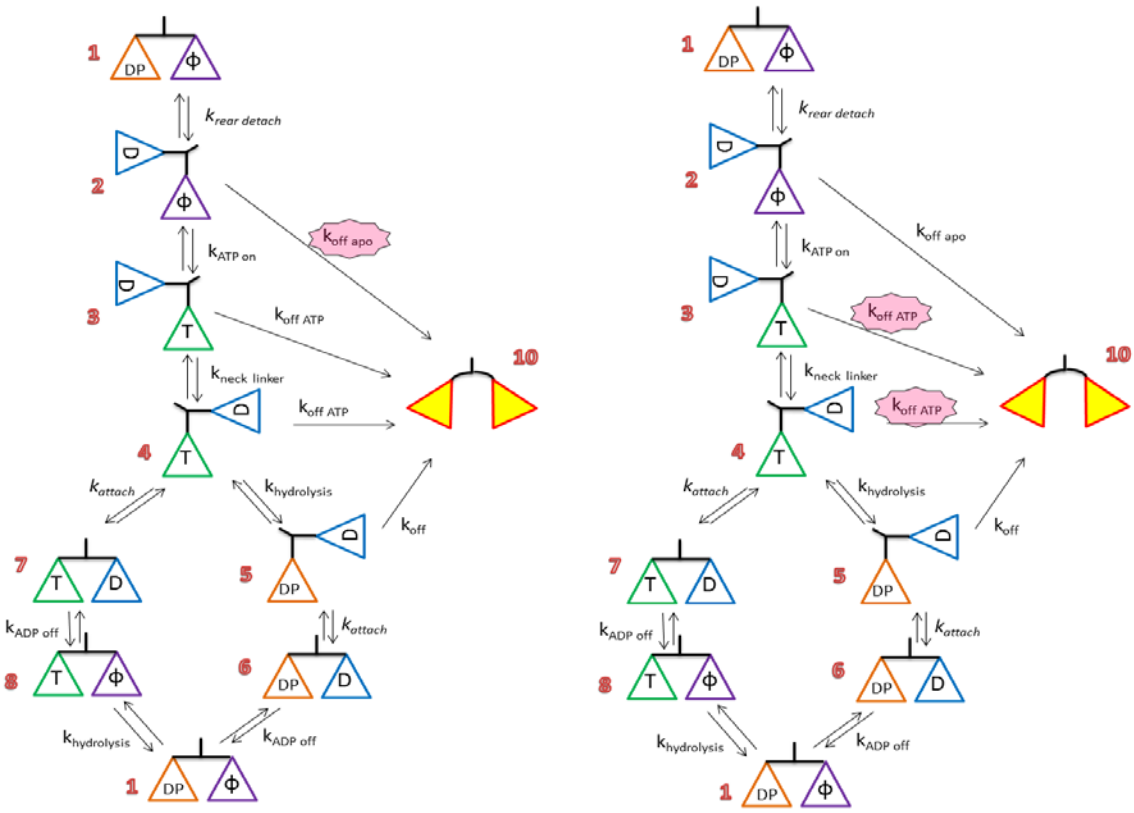

Figure 19: Chemomechanical pathway highlighting apo and ATP dissociation rates

A. A possible dissociation route from the no nucleotide (apo) state is highlighted.
B. Possible dissociation routes from the ATP-bound state, before and after neck linker docking, is highlighted in the chemomechanical pathway.

Chapter 4

Experimental Evidence

To help reject or support the alternate pathway with rear-head attachment preceding hydrolysis, the dissociation rates of kin-5 in states that are considered to be strongly bound to the microtubule were determined. If kin-5 with no nucleotide or with ATP demonstrated a significant dissociation rate, then the alternate hydrolysis pathway could explain the low processivity of kin-5.

Although there are some data on the dissociation rates of various nucleotides [41, 43, 42], the dissociation rate constants have been studied much more for kin-1 than for kin-5. Also, the constructs used in literature are different than those in the assays reported here. These rate constants were crucial for the simulations, especially when considering the novel hydrolysis pathway.

The following assays used an engineered human Eg5 dimer truncated after the neck linker at position 553 and attached to a kinesin-1 *Drosophilia* coiled-coil with a C-terminal GFP. This was a stable and well-characterized coiled-coil with successful dimerization in previous studies [13].

Methods – Pelleting Assay

A pelleting assay was performed to characterize the dissociation rate of ADP-bound motors. The assay measures the fraction of motors that are bound to microtubules at equilibrium at varying microtubule concentrations, so the K_d can be

determined. From attachment rates (k_{on}) calculated by ATPase assays and the resulting K_d, the dissociation rate (k_{off}) can be calculated.

The GFP kin-5 concentration was held constant at 0.01 μM while the microtubule concentration varied up to 10 uM. The motor protein was incubated with the microtubules for 10 minutes at room temperature and centrifuged in a Beckman Airfuge at 30 psi for 10 minutes, sufficient to pellet the microtubules and any attached motors. The supernatant was removed, and the pellet was resuspended in BRB80. The fluorescence of the pre-spin sample, supernatant, and pellet were determined using a Shimadzu Spectrofluorometer, exciting at 488 nm and collecting emission between 505 and 545 nm. The peak intensity of the resulting emission curve correlated to the kin-5 concentration in the sample.

The pellet is the concentration of kinesin that bound to the microtubule. However, there were discrepancies in the pellet data at higher microtubule concentrations that could have been caused by quenching or light scattering by the microtubules; this did not affect the supernatant since the concentration of microtubules was lower. Therefore, only the supernatant and pre-spin samples were further analyzed, assuming that pre-spin = supernatant + pellet.

A sample without microtubules was used to normalize for no binding, and the ratio of the supernatant intensity against the pre-spin intensity was used to adjust for inconstancies in motor protein concentrations throughout the samples. The raw data and normalized values of the supernatant were plotted against microtubule concentration and fit to a binding isotherm.

$$[\mathrm{Mt}] + [\mathrm{Kin}] \underset{k_{off}}{\overset{k_{on}}{\longleftrightarrow}} [\mathrm{MtKin}]$$

$$[\mathrm{MtKin}] = \frac{[K_{active}][\mathrm{Mt}]}{K_d + [\mathrm{Mt}]}$$

The curve was fit in MATLAB with a built-in algorithm using the equation

$$y = \frac{c_1 * x}{c_2 + x}$$

that corresponds to the variables in the equation above.

The attachment rate was determined by a stopped-flow experiment. The dissociation rate could be calculated, as

$$K_d = \frac{k_{off}}{k_{on}}$$

Pelleting Assay Discussion & Results

A pelleting, or cosedimentation, assay was used to characterize the dissociation constant of the ADP-bound state. Table 10 shows the mean K_d was 0.45 μM using data from the supernatant adjusted to the pre-spin. Figure 22 shows the mean k_{on} from ATPase assays was 5.2 $\mu M^{-1}s^{-1}$. Table 10 provides the K_d and k_{off} values from the pelleting assay. The k_{off} for ADP is around 12 s^{-1}. This was very close to the reported values of 8-10 s^{-1} [42, 43], which were used in the computational models. The difference may be due to the assumption that the supernatant was not affected by the GFP or microtubules at high concentrations, like the pellet. The intensities continued to increase slightly at high microtubule concentrations, as shown in Figure 20.

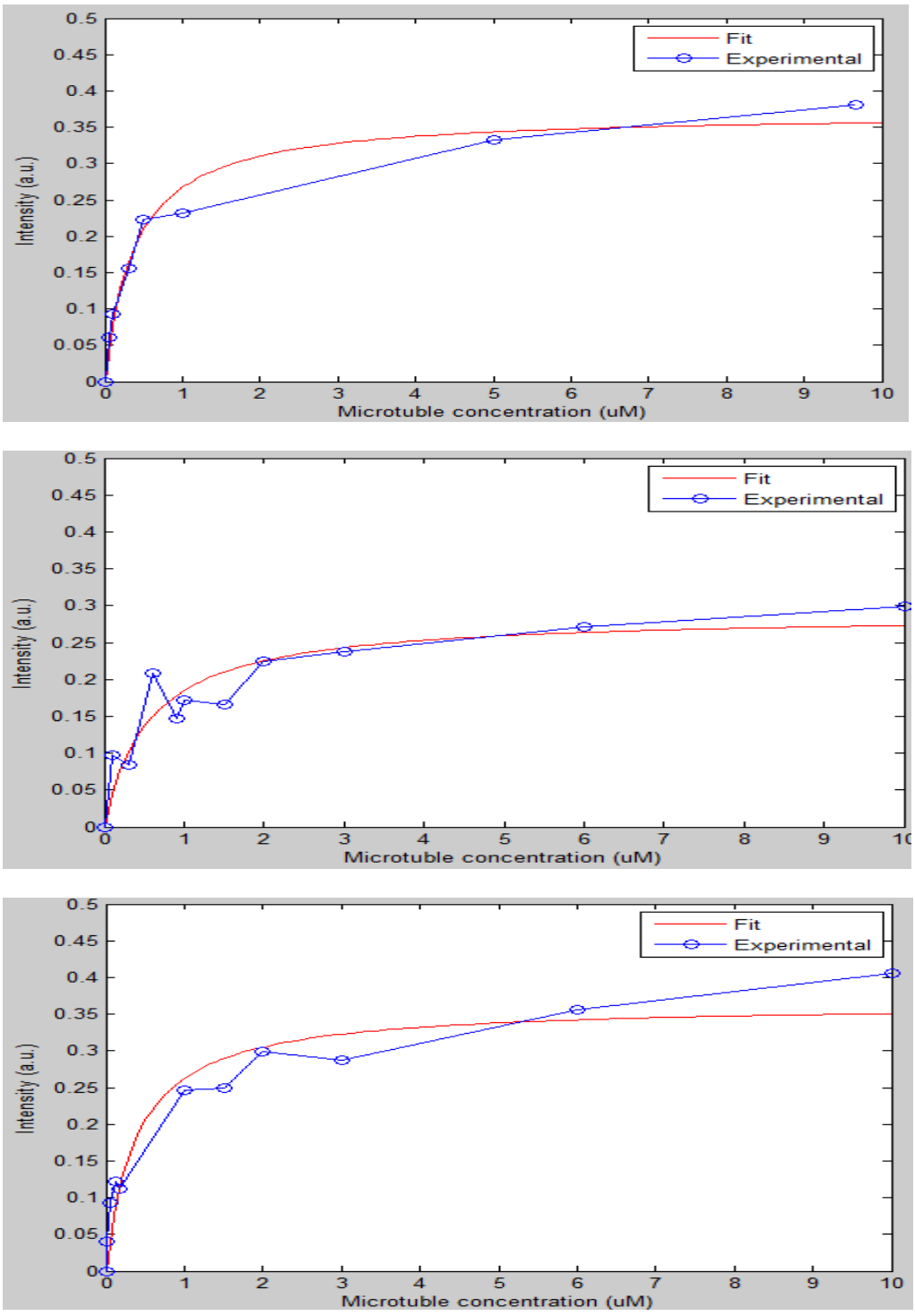

Figure 20: Binding isotherms of kin-5 with ADP

The fluorescence intensity of the supernatant was adjusted to the pre-spin samples and transformed into a binding isotherm that followed Machaelis-Menten kinetics. The resulting K_ds were 0.39, 0.56, 0.39 µM, averaging to 0.45 µM and providing a mean ADP dissociation rate of approximately 12 s^{-1}.

Table 9: Active kin-5 motor concentration from binding isotherm

Trial	% Active motors
1	37
2	29
3	36
Average	34

Table 10: ADP K_d and k_{off} from binding isotherm

Trial	K_d (µM)	k_{off} (s^{-1})
1	0.39	13.6
2	0.56	9.5
3	0.39	13.6
Average	0.45	**12.2**

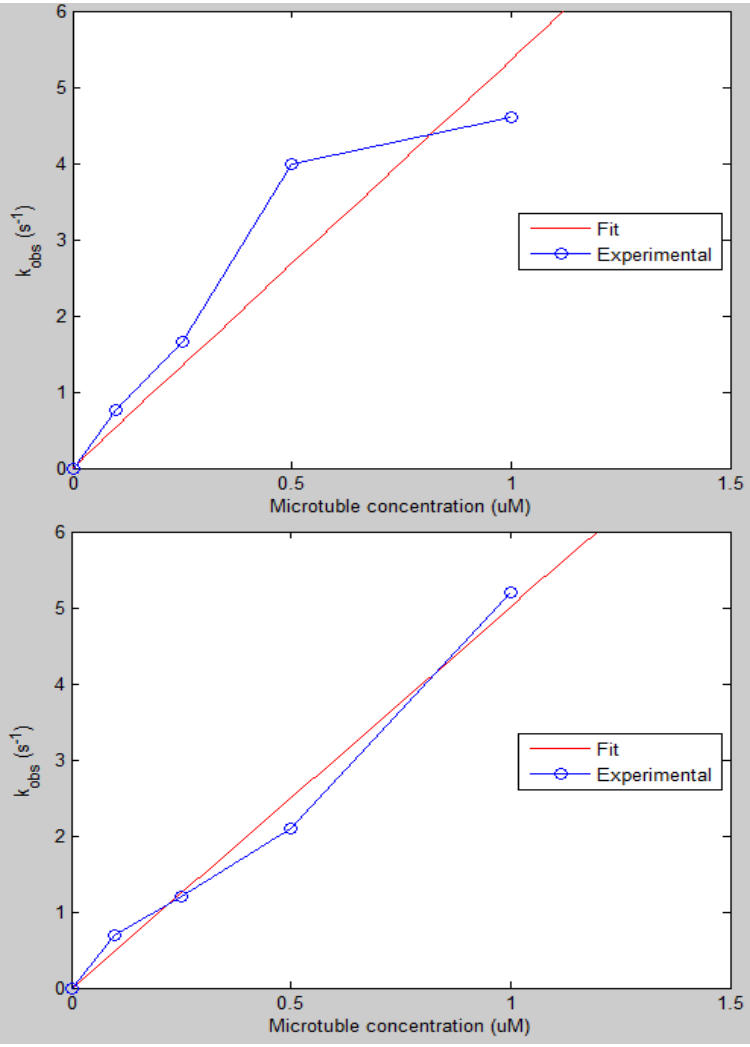

Figure 21: Attachment rates from ATPase assay

A stopped flow assay by Dr. Hancock measured the rate of kin5-14 with ADP binding to microtubules. Motors were incubated in mantADP so that both heads had bound mantADP. These motors were then flushed against varying concentrations of microtubules containing 10 µM cold ADP. Binding of motors to microtubules led to release of mantADP,

with the cold ADP preventing any rebinding of mantADP to the motors. The reaction consisted of a microtubule binding step followed by a mantADP release step. Hence, at low microtubule concentrations, this assay can be used to measure the binding rate to microtubules. These data were combined with K_d measurements from microtubule pelleting experiments to estimate the detachment rate of kin-5 motor in the ADP state (k_{on}). Two experiments were run with attachment rates of 5.0 $\mu M^{-1}s^{-1}$ and 5.3 $\mu M^{-1}s^{-1}$.

METHODS – FLUORESCENCE MOTOR DISSOCIATION ASSAY

While the microtubule pelleting assay worked for the low affinity ADP state, measurements of high affinities (low K_d) in the assay is hampered by problems with motor crowding. At limiting microtubule concentrations, the number of motors that pellet is limited by the number of tubulin binding sites and not by the K_d. Hence, a fluorescence assay was used to determine the upper limit of dissociation rates of kin-5 in different nucleotide states. Microtubules were introduced into a flow cell and allowed to absorb via α-tubulin antibody. Excess kin-5 with GPF with either AMP-PNP or no nucleotide was added into the flow cell and allowed to bind to the microtubules. Motors with AMP-PNP were bound to the microtubules with both heads, and motors with no nucleotide were bound with one head [52, 48]. Any unbound motors were washed out and all of the remaining motors were bound to microtubules. The motors were viewed by fluorescence microscopy, and microtubules were introduced to the flow cell. AMP-PNP used a laser power of 1.5 mA with a 2x neutral density filter due to the bright GFP signal. Motors with no nucleotide used 10 mA laser power with no filter, providing brighter illumination. STK movies were recorded with frame rates of 250 ms for AMP-PNP and 1 s for no nucleotide.

The images were analyzed with ImageJ with the Time Series Analyzer plug-in. Samples in four regions were taken that included a small area (approx. 10 x 40 pixels) of a microtubule, and the average intensity was measured for each frame. Background samples of a much larger area containing no microtubule were also

measured. The background samples were averaged, then subtracted from the microtubule samples, frame-by-frame, to adjust for noise, including Johnson-Nyquist noise, stray light, and any other error sources from the microscope.

The observed intensity change was due to dissociating from the microtubules and photobleaching. Thus, if any photobleaching occurred, the dissociation rate would be an unknown amount less than or equal to the observed rate. If the photobleaching was negligible compared to the dissociation ($k_{bleach} \approx 0$), then the observed rate would be the largest possible dissociation constant.

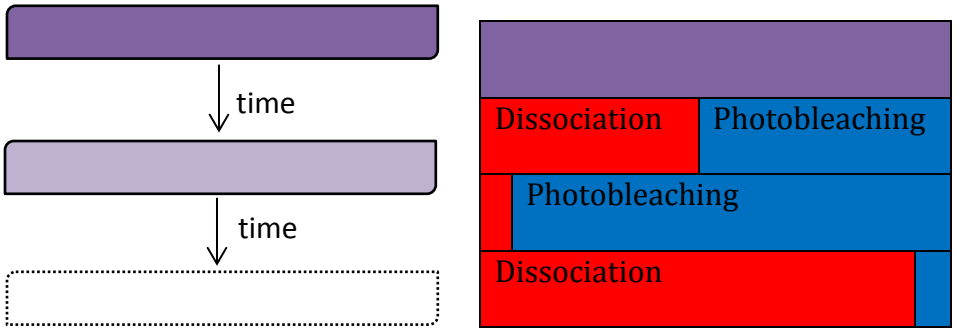

Figure 22: Dissociation and photobleaching combinations

A. The fluorescence of motor proteins observed decreased exponentially with time until it eventually blended with the background. Instances where the fluorescence did not appear to decrease can be assumed to be at time zero.

B. The observed fluorescence is a combination of dissociation and photobleaching. It can be any combination of the two: a semi-even split, mostly photobleaching, or mostly dissociation. The dissociation rate cannot be more than the observed rate.

Using ImageJ, the adjusted data was fitted to an exponential curve of form

$$y = ae^{-k_{obs}t}$$

where *a* is the initial amplitude in arbitrary units and *k* is the observed rate constant in s^{-1}. Since k_{obs} is a summation of photobleaching and dissociation, the actual equation is

$$y = ae^{-(k_{dissoc.}+k_{bleach})t}$$

For instances where the intensity did not significantly decrease throughout the movie, it was assumed that the intensity change followed the same exponential equation but only the initial decrease was observed. Although the experimental time was several minutes long, it was analyzed at time zero relative to the time it would take for the intensity to decrease to the background values, such that

$$\frac{dy}{dt} = -ak_{obs}e^{-k_{obs}t}, \ \ at\ t = 0, \ \ \frac{dy}{dt} = -ak_{obs}$$

The derivative of the intensity $\frac{dy}{dt}$ is equal to the linear slope of fluorescence/time and the amplitude can be measured with the initial data points, allowing *k* to be calculated algebraically.

FLUORESCENCE DISSOCIATION ASSAY DISCUSSION & RESULTS

The motor dissociation assay was used to determine the upper limit of the microtubule dissociation rate of the apo and ATP-bound states by measuring the decrease in fluorescence intensity over the assay time.

The apo state was analyzed with four microtubule samples and three background samples. The results are shown in Table 11. The upper bound for dissociation in the apo state was 0.013 s^{-1}, meaning that the motor would remain in the apo state for over a minute before it dissociates from the microtubule.

Table 11: Amplitudes and rate constants for apo state

The curve follows the formula $y = ae^{-kt}$. The upper limit of dissociation for the apo state is $0.013s^{-1}$.

Sample	A (a.u.)	k (s^{-1})
1	4594	0.012
2	2521	0.012
3	3122	0.014
4	4068	0.013
Average	3576	0.013
Std. Dev.	931	0.001

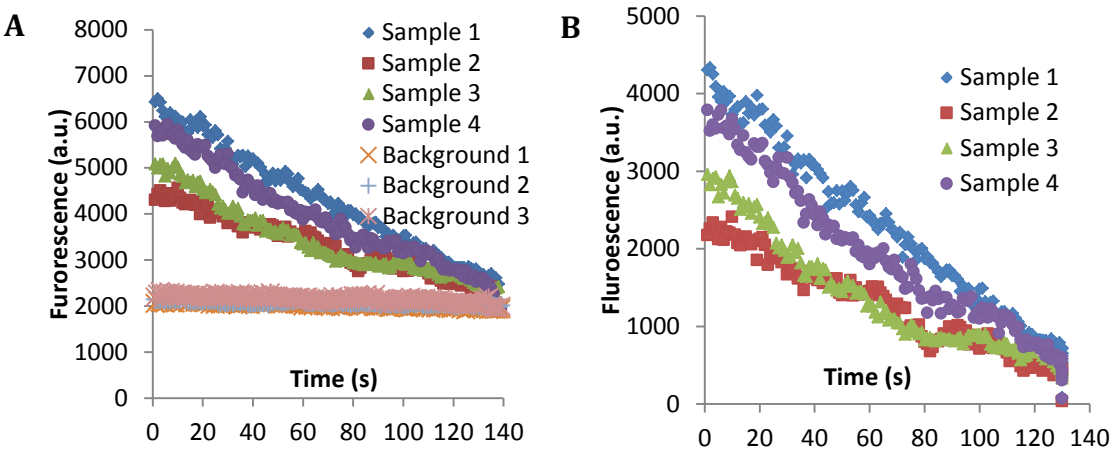

Figure 23: Apo state dissociation curve

A. Data from the fluorescence dissociation assay, including the background samples. The background includes Johnson-Nyquist noise, stray light, and other constant noise from the microscope.
B. Data, adjusted for background noise, follows an exponential with a slow rate, appearing almost linear. The decrease in fluorescence is due to the cumulative effects of photobleaching and dissociation.

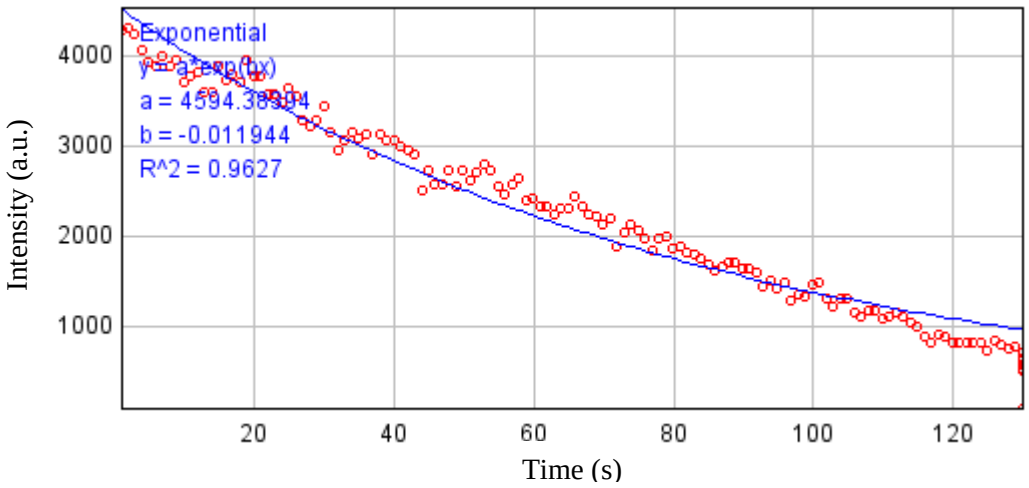

Figure 24: Dissociation and photobleaching curve for apo Sample #1

Each normalized sample was fit to an exponential dissociation curve. This shows the parameters for the amplitude (4594) and the exponential constant (0.012 s^{-1}) for sample #1.

The ATP-bound state was analyzed using AMP-PNP, a non-hydrolysable ATP analog. The fluorescence was stronger, and the fluorescence intensity nearly remained constant during the experiment, exhibiting minimal dissociation or photobleaching. The minimal photobleaching is due to lower laser excitation and no neural density filter, which was enabled by the brighter fluorescence of the AMP-PNP sample. Therefore, the results were analyzed differently. The upper limit of dissociation is about 0.0003 s^{-1}, which gives a maximum time before dissociation of one hour!

Table 12: Amplitudes and rate rate constants for ATP state

Sample	a (a.u.)	*m (a.u.*s^{-1})*	*k* (s^{-1})
1	8606	1.88	0.00022
2	9619	3.89	0.00040
3	4174	0.93	0.00022
4	6710	1.84	0.00028
Average			0.00028
Std. Dev.			0.00008

Analyzed as a line at t=0, the curve follows the formula $m = ak$. Although the range of amplitudes and slopes is large, the constant, k, remains within 2-4 x 10^{-4} s^{-1}. k is a combination of photobleaching and dissociation.

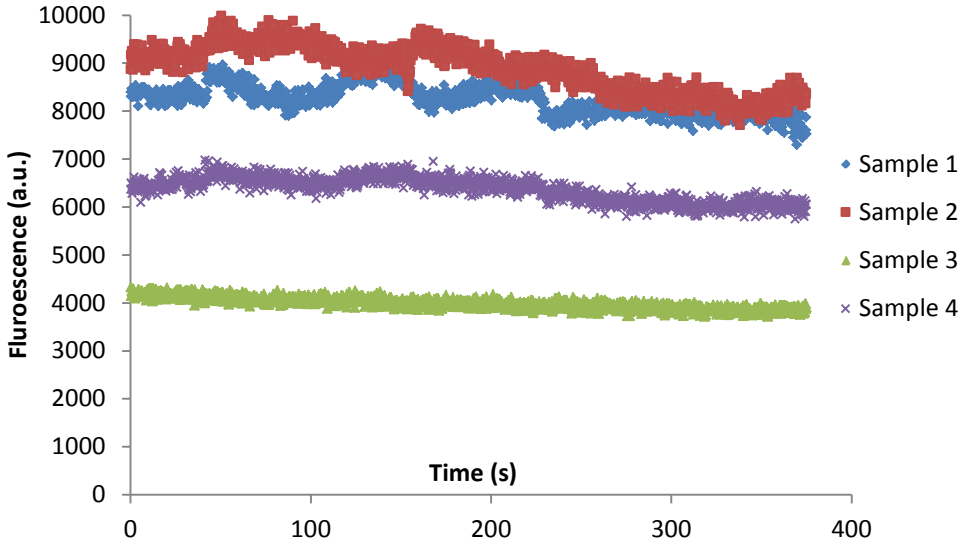

Figure 25: AMP-PNP dissociation curve

The AMP-PNP data for photobleaching and dissociation barely decreased from the initial value throughout the experiment.

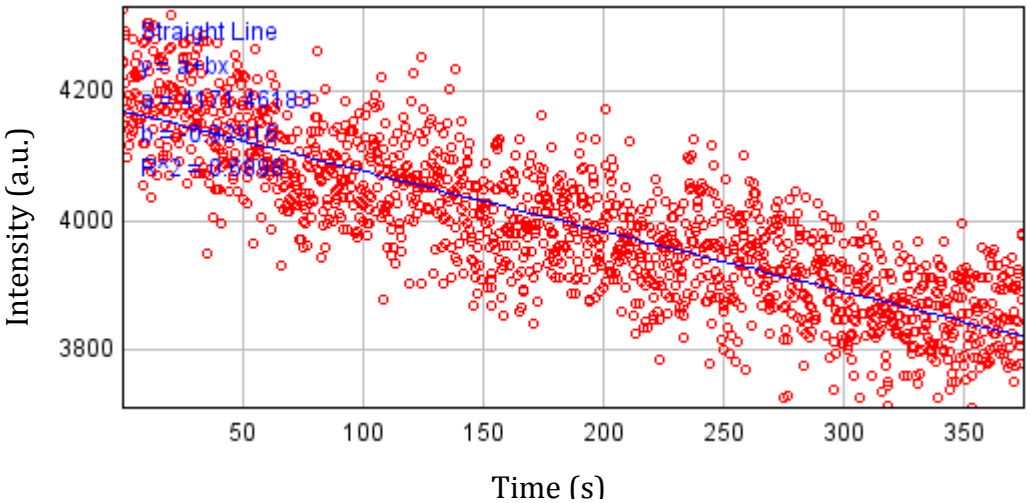

Figure 26: Dissociation and photobleaching curve for AMP-PNP Sample #3

The rate of dissociation and photobleaching for AMP-PNP was fit to a linear curve due to the minimal change in amplitude. Sample #3 had an amplitude of 4174 (a.u.) and a slope of 0.93 a.u.*s, thus the rate is 0.00022 s^{-1}.

Chapter 5
Conclusions and Future Studies

The consensus pathway was analyzed with values found in literature. In a pathway with seven states, including the unattached state, the rate constants were analyzed to determine which constants most significantly affected the velocity. Based on the values provided in the literature by two different labs and empirically adjusting the attachment rate to achieve a run length of 64 nm, the maximum unloaded velocities possible are between 20 nm/s and 35 nm/s, much lower than the observed values of 100 nm/s. This result can be explained by the literature values showing the pathway limited by two steps: rear-head detachment and ATP hydrolysis. Thus, kin-5 velocities predicted from the rate constants in the literature do not agree with the experimentally determined velocities.

A new pathway was created for analysis that included front- and rear-head gating and a novel hydrolysis pathway where attachment occurred before ATP hydrolysis. The simulation also modeled the neck linker domain as a worm-like chain with interhead strain that affected the rear-head detachment rate and the tethered-head attachment rate. However, the modeled rates from shortening the neck linker had opposite effects on the processivity than the experimentally measured run lengths, and interhead strain was not considered in the following models.

The pathway with tethered-head attachment preceding hydrolysis lacked the ADP-bound state that provided the primary chance of dissociation. To help reject or

support the alternate pathway, the minimum dissociation rates were determined for the no nucleotide and ATP-bound states by forcing the motor to take the alternate pathway and have a run length of approximately eight steps.

The apo, ATP-bound, and ADP-bound states were reexamined to determine whether kin-5 was strongly bound to the microtubule in these states. The dissociation rates of kin-5 were studied with fluorescence and pelleting assays and compared to the simulation values.

The dissociation rate from the simulations necessary to match experimentally determined run lengths from the simulations was 140 s^{-1}. Although this value is of the same order of magnitude as the other rates, it is 10,000 fold larger than the experimental value of 0.013 s^{-1} determined by the fluorescence dissociation assay. Hence, the simulated ATP-bound rate was only 7 s^{-1}. However, the experimental value from the fluorescence dissociation assay was only 0.0003, so this is 20,000 fold larger. The ADP-bound dissociation rate was 9 s^{-1} in literature and determined to be 12 s^{-1} from the pelleting and stopped flow assays; both of these values confirm it as a weakly-bound state.

The high processivity from the simulations with the alternate hydrolysis pathway and the low dissociation rates for strongly bound states provides evidence rejecting the chemomechanical pathway with hydrolysis after tethered-head attachment. The processivity increase associated with shorter neck linker lengths was inconclusive by modeling the neck linker as a worm-like chain.

SUGGESTED FUTURE WORK

Most of the analysis ignored the velocity data since it was impossible to be much above 40 nm/s using rate constants from the literature. However, the question on the rate-limiting step is not completely answered. Obtaining accurate data on the rates of hydrolysis and rear-head detachment would help eliminate this discrepancy. More information on hydrolysis would also provide insight if the alternate hydrolysis pathway is a possibility.

There were no experiments performed to study whether gating occurs with kin-5. This could be tested by measuring the processivity in varying concentration of available ATP, as explained in Muthukrishnan et al [36]. In low ATP concentrations, the motor would favor rear-head gating (the consensus pathway) and have a lower processivity; in high ATP concentrations, the front-head gating pathway would be more likely, so the motor would show longer run lengths.

A model explaining the increase in processivity with a decrease in neck linker length has yet to be determined. Structural data from crystallography and cryo-electron microscopy with MD simulations may provide deeper insight into the mechanism behind the phenomenon.

Although the experiments used a human kin-5, all of the assays were performed *in vitro*. A full-length construct resistant to a sample of si-RNA was created by Dr. Ryoma Ohi at Vanderbilt University. Information on the effects of the neck linker length could be obtained by modifying the construct by removing the last four amino acids in the neck linker. According to Shastry and Hancock, the

construct should behave like kin-1 *in vitro* [12]. The construct and the si-RNA can be inserted in a mammalian cell, and the natural kin-5 would be destroyed. The effects of a more processive and more rapid kin-5 could be analyzed most directly by measurements on the mammalian mitotic spindle formation and chromosome segregation during anaphase. Efforts to create the modified construct were unsuccessful this far (See Appendix A for details on the molecular biology).

Appendix A

Generation of an Engineered Kin-5

Plasmids were obtained from Dr. Ryoma Ohi in Vanderbilt University Medical Center for human kin-5. They were Kanamycin-resistant in a pDGFP-N! plasmid from Clontech. The plasmid design was modified using Vector NTI suite to shorten the natural 18 amino acid neck linker domain to 14 amino acids, removing 12 nucleotides. The removal was being attempted using Stratagene's Quick-Change II XL site-directed mutagenesis kit in two rounds (removing 6 nucleotides each time) using E. coli(XL-10 Gold super-competent cells). Unfortunately, the Quick-Change was unsuccessful with molecular biology issues occurring in the transformation process

REFERENCES

[1] A. Lockhart and R. A. Cross, “Kinetics and motility of the Eg5 microtubule motor,” *Biochem,* vol. 35, pp. 2365-2373, 1996.

[2] H. Miki, Y. Okada and N. Hirokawa, “Analysis of the kinesin superfamily insights into structure and function,” *Trends Cell Biol,* vol. 15, no. 9, pp. 467-476, Sep 2005.

[3] B. H. Kwok, L. C. Kapitein, J. H. Kim, E. J. Peterman, C. F. Schmidt and T. M. Kapoor, “Allosteric inhibition of kinesin-5 modulates its processive directional motility,” *Nat Letters Chem Biol,* vol. 2, no. 9, pp. 480-485, Sep 2006.

[4] F. Kozielski, S. Sack, A. Marx, M. Thormahlen, E. Schonbrunn, V. Biou, A. Thompson, E. M. Mandelkow and E. Mandelkow, "The crystal structure of dimeric kinesin and implications for microtubule-dependent motility," *Cell,* vol. 91, no. 7, pp. 985-994, 1997.

[5] S. M. Block, "Kinesin motor mechanics: Binding, stepping, tracking, gating, and limping," *Biophys,* vol. 92, pp. 2986-2995, 2007.

[6] B. E. Clancy, W. M. Behnke-Parks, J. O. L. Andreasson, S. S. Rosenfeld and S. M. Block, "A universal pathway for kinesin stepping," *Nature,* vol. 18, no. 9, pp. 1020-1027, 2011.

[7] T. C. Crevel, A. Lockhart and R. A. Cross, “Kinetic evidence for low chemical processivity in ncd and Eg5,” *J Mol Biol,* vol. 273, pp. 160-170, 1997.

[8] W. O. Hancock and J. Howard, "Processivity of the motor protein kinesin requires two heads," *J Cell Biol,* vol. 140, no. 6, pp. 1395-1405, 1998.

[9] B. J. Schnapp, T. S. Reese and R. Bechtold, "Kinesin is bound with high affinity to squid axon organelles that move to the plus-end of microtubules," *J. Cell Biol.,* vol. 119, no. 2, pp. 389-399, 1992.

[10] K. H. Downing and E. Nogales, "Tubulin and microtubule structure," *Curr. Opinion Cell Biol.,* vol. 10, pp. 16-22, 1998.

[11] N. Hirokawa, "Kinesin and dynein superfamily proteins and the mechanism of organelle transport," *Science,* vol. 279, pp. 519-526, 1998.

[12] M. T. Valentine and S. M. Block, "Force and premature binding of ADP can regulate the processivity of individual Eg5 dimers," *Biophys. J,* vol. 97, pp. 1671-1677, 2009.

[13] S. Shastry and W. O. Hancock, “Interhead tension determines processivity across diverse N-terminal kinesins,” *Proc. Natl. Acad. Sci.,* vol. 108, no. 39, pp. 16253-16258, 2011.

[14] D. D. Hackney, "Evidence for altering head catalysis by kinesin during microtubule-stimulated ATP hydrolysis," *Proc. Natl. Acad. Sci.,* vol. 91, no. 15, pp. 6865-6869, 1994.

[15] S. Shastry and W. O. Hancock, “Neck linker length determines the degree of processivity in kinesin-1 and kinesin-2 motors,” *Curr Biol,* vol. 10, no. 25, pp. 939-943, 2010.

[16] N. J. Carter and R. A. Cross, "Mechanics of the kinesin step," *Nature,* vol. 435, no. 19, pp. 308-312, 2005.

[17] S. S. Rosenfeld, P. M. Fordyce, G. M. Jefferson, P. H. King and S. M. Block, "Stepping and stretching: How kinesin uses internal strain to walk processively," *J. Biol. Chem.,* vol. 278,

pp. 18550-18556, 2003.

[18] A. Yildiz, M. Tomishige, A. Gennerich and R. D. Vale, "Intramolecular strain coordinates kinesin stepping behavior along microtubules," *Cell,* vol. 134, pp. 1030-1041, 2008.

[19] D. D. Hackney, "The teathered motor domain of a kinesin-microtubule complex catalyzes reversible synthesis of bound ATP," *PNAS,* vol. 102, no. 51, pp. 18338-18343, 2005.

[20] R. A. Cross, "The kinetic mechanism on kinesin," *Trends Biochem Sci,* vol. 29, no. 6, pp. 301-309, 2004.

[21] K. Homma and M. Ikebe, "Myosin X is a high duty ratio motor," *J Biol Chem,* vol. 280, pp. 29381-29391, 2005.

[22] J. Howard, "Molecular motors: Structural adaptations to cellular functions," *Nature,* vol. 389, pp. 561-567, 1997.

[23] T. Q. Uyeda, S. J. Kron and J. A. Spudich, "Myosin step size: Estimation from slow sliding movement of actin over low densities of heavy meromyosin," *J. Molec. Biol.,* vol. 214, no. 3, pp. 699-710, 1990.

[24] D. E. Harris and D. M. Warshaw, "Smooth adn skeletal msucle myosin both exhibit low duty cycles at zero load in vitro," *J. Biol. Chem.,* vol. 268, no. 20, pp. 14764-1468, 1993.

[25] L. C. Kapitein, B. H. Kwok, J. S. Weinger, C. F. Schmidt, T. M. Kapoor and E. J. Paterman, "Microtubule cross-linking triggers the directional motility of kinesin-5," *J Cell Biol,* vol. 182, no. 3, pp. 421-428, 2008.

[26] L. C. Kapitein, E. J. Peterman, B. H. Kwok, J. H. Kim, T. M. Kapoor and C. F. Schmidt, "The bipolar mitotic kinesin Eg5 moves on both microtubules that it crosslinks," *Nature Letters,* vol. 435, no. 7038, pp. 114-118, May 2005.

[27] M. Gartner, N. Sunder-Plassmann, J. Seiler, M. Utz, I. Vernos, T. Surrey and A. Giannis, "Development and biological evaluation of potent and specific inhibitors of mitotic kinesin Eg5," *Chem Bio Chem,* vol. 6, pp. 1173-1177, 2005.

[28] N. L. Craig, O. Cohen-Fix, R. Green, C. w. Greider, G. Storz and C. Wolberger, "Chapter 7: Chromosome Segregation," in *Molecular Biology: Principles of Genome Function,* New York, Oxford University Press, 2010, pp. 255-257.

[29] I. Brust-Mascher and J. M. Scholey, "Mitotic motors and chromosome segregation: the mechanism of anaphase B," *Cellular Cytoskeletal Motor Proteins,* vol. 35, pp. 1149-1153, 2011.

[30] I. Brust-Mascher and J. M. Scholey, "Microtubule flux and sliding in mitotic spindles of Drosophilia embroyos," *Molec Biol Cell,* vol. 13, pp. 3967-3975, 2002.

[31] M. T. Valentine, P. M. Fordyce, T. C. Krzysiak, S. P. Gilbert and S. M. Block, "Individual dimers of the mitotic kinesin motor Eg5 step processively and support substantial loads in vitro," *Nat Letters Cell Biol,* vol. 8, no. 5, pp. 470-476, 2006.

[32] K. J. Skowronek, E. Kocik and A. A. Kasprzak, "Subunits ineteractions in kinesin motors," *European J. Cell Biol.,* vol. 86, no. 9, pp. 559-568, 2007.

[33] S. S. Rosenfeld, J. Xing, G. M. Jefferson and P. H. King, "Docking and rolling, a model of how the mitotic motor Eg5 works," *J Biol Chem,* vol. 280, no. 42, pp. 35684-35695, 2005.

[34] D. A. Benson, I. Karsch-Mizarchi, D. J. Lipman, J. Ostell and D. L. Wheeler, "GenBank," *Nucleic Acids Res.,* vol. 34, p. Database Issue, 2006.

[35] R. B. Case, S. Rice, C. L. Hart, B. Ly and R. D. Vale, "Role of the kinesin neck linker and catalytic core in microtubule-based motility," *Curr Biol,* vol. 10, no. 3, pp. 157-160, 2000.

[36] W. R. Hesse, M. Steiner, M. L. Wohlever, R. D. Kamm, W. Hwang and M. J. Lang, "Modular aspects of kinesin force generation machinery," *Biophys. J.*, vol. 104, pp. 1969-1978, 2013.

[37] G. Muthukrishnan, Y. Zhang, S. Shastry and W. O. Hancock, "The processivity of kinesin-2 motors suggests diminished front-head gating," *Curr Biol*, vol. 19, pp. 442-447, 2009.

[38] T. U. Mayer, T. M. Kapoor, S. J. Haggarty, R. W. King, S. L. Schreiber and T. J. Mitchison, "Small molecule inhibitor of mitotic spindle bipolarity identified in phenotype-based screen," *Science*, vol. 286, no. 5441, pp. 971-974, 1999.

[39] J. Jaworski, L. C. Kapitein, S. M. Gouveia, B. R. Dortland, P. S. Wulf, I. Grigoriev, P. Camera, S. A. Spangler, P. DiStefano, J. Demmers, H. Krugers, P. Defilipppi, A. Akhmanova and C. C. Hoogenraad, "Dynamic microtubules regulate dendritic spine morphology and synaptic plasticity," *Neuron*, vol. 61, pp. 85-100, 15 Jan 2009.

[40] S. DeBonis, D. A. Skoufias, L. Lebeau, R. Lopez, G. Robin, R. L. Margolis, R. H. Wade and F. Kozielski, "In vitro screening for inhibitors of the human mitotic kinesin Eg5 with antimittic and antitumor activities," *Mol Cancer Therapeutics*, vol. 3, pp. 1079-1090, 2004.

[41] "Monastrol - Compound Summary," NCBI, 25 Mar 2005. [Online]. [Accessed Apr 2013].

[42] W. M. Behnke-Parks, J. Vendome, B. Honig, Z. Maliga, C. Moores and S. S. Rosenfeld, "Loop L5 acts as a conformational latch in the mitotic kinesin Eg5," *J. Cell Biol*, vol. 286, no. 7, pp. 5242-5253, 2011.

[43] T. C. Krzysiak and S. P. Gilbert, "Dimeric Eg5 maintains processivity through alternating-site catalysis with rate-limiting ATP hydrolysis," *J Biol Chem*, vol. 281, no. 51, pp. 39444-39454, 2006.

[44] T. C. Krzysiak, M. Graba and S. P. Gilbert, "Getting in sync with dimeric Eg5: Initiation adn regulation of the processive run," *J Biol Chem*, vol. 283, no. 4, pp. 2078-2087, 2008.

[45] D. T. Gillespie, "Exact stochastic simulation of coupled chemical reactions," *J Phys Chem*, vol. 81, no. 25, pp. 2340-2381, 1977.

[46] M. L. Kutys, J. Fricks and W. O. Hancock, "Monte Carlo analysis of neck linker extension in kinesin molecular motors," *PLoS Computational Biology*, vol. 6, no. 11, pp. 1-11, 2010.

[47] G. I. Bell, "Models for hte sepcific adhisesion of cells to cells," *Science*, vol. 220, no. 4342, pp. 618-627, 1978.

[48] K. Kawaguchi, S. Uemura and S. Ishiwata, "Equilibrium and transition between single- and double-headed binding of kinesin as revealed by single-molecule mechanics," *Biophys. J*, vol. 84, pp. 1103-1113, 2003.

[49] P. Ghosh, Stochastic Models for In-silico Event-based Biological Network Simulation, Ann Arbor, MI: ProQuest Information and Learning Company, 2008, pp. 56-57.

[50] M. T. Valentine and S. P. Gilbert, "To step or not to step? How biochemistry and mechanics influence processivity in Kinesin and Eg5," *Curr Opinion Cell Biol*, vol. 19, pp. 75-81, 2007.

[51] Y.-Z. Ma and E. W. Taylor, "Interacting head mechanism of microtubule-kineesin ATpase," *J. Biol. Chem.*, vol. 272, no. 2, pp. 724-730, 1997.

[52] S. Uemura, K. Kawaguchi, J. Yajima, M. Edamatsu, Y. Y. Toyoshima and S. Ishiwata, "Kinesin-microtubule binding depends on both nucleotide state and loading direction," *Proc. Natl. Acad. Sci.*, vol. 99, no. 9, pp. 5977-5981, 2002.

[53] J. C. Cochran, C. A. Sontag, Z. Maliga, T. M. Kapoor, J. J. Correia and S. A. Gilbert, "Mechanistic analysis of the mitotic kinesin Eg5," *J Biol Chem*, vol. 279, no. 37, pp. 38861-38870, 2004.

[54] A. n. Fehr, B. Gutierrez-Medina, C. L. Asbury and S. M. Block, "On the origin of kinesin limping," *Biophys*, vol. 97, pp. 1663-1670, 2009.

[55] C. L. Asbury, A. N. Fehr and S. M. Block, "Kinesin moves by an asymmetric hand-over-hand mechanism," *Science*, vol. 302, pp. 2130-2134, 2003.

[56] S. Rice, A. W. Lin, D. Safer, C. L. Hart, N. Naber, B. O. Carragher, S. M. Cain, E. Pechatnikova, E. M. Wilson-Kubalek, M. Wittaker, E. Pate, R. Cooke, E. W. Taylor, R. A. Milligan and R. D. Vale, "A structural change in the kinesin motor protein that drives motility," *Nature*, vol. 402, pp. 778-784, 1999.

[57] V. Hariharan and W. O. Hancock, "Insights into the mechanical properties of hte kinesin neck lnker from sequence analysis and molecular dynamics simulations," *Cell and Molec Bioeng*, vol. 2, no. 2, pp. 177-189, 2009.

[58] M. Tomishige, "Activation of mitotic kinesin by microtubule bundling," *J Cell Biol*, vol. 182, no. 3, pp. 417-419, 2008.

[59] G. Piazzesi, M. Reconditi, M. Linari, L. Lucii, Y.-B. Sun, T. Narayanan, P. Boesecke, V. Lombardi and M. Irving, "Mechanism of force generation by myosin heads in skeletal muscle," *Letters to Nature*, vol. 415, pp. 659-662, 2002.

M. T. Valentine, P. M. Fordyce and S. M. Block, "Eg5 steps it up!," *Cell Division*, vol. 1,
60] no. 31, 2006.

ACADEMIC VITA

Tiffany L. Senkow
senkowt@gmail.com

Education

B.S., Bioengineering, 2013, The Pennsylvania State University, State College, PA
School of Language and Culture for Foreigners, 2010, Kraków, Poland

Honors and Awards

South Dakota REU in Alternative Energy	Summer 2012
Penn State REU in Soft Materials in Material Science	Summer 2011
Behrend Summer Research Fellowship	Summer 2010
Remkus-Sochakus Academic Fellowship	Fall 2011 – Spring 2013
Schreyer Honors College Academic Excellence Scholarship	Fall 2009 – Spring 2013
Dean's List	Fall 2009 – Spring 2013

Research experience

Research Assistant; Penn State University, University Park, PA Spring 2013 - Present
Department of Bioengineering
Professor William Hancock

Mechanism and Kinetics of Human Kinesin-5

- Modeled chemo-mechanical pathways of motor proteins in MATLAB
- Created mutants and performed assays to determine rate constants

Research Assistant; South Dakota State University, Brookings, SD Summer 2012
Department of Microbiology
Professor Thomas West

Biopolymer Production using Plant Biomass

- Isolated fungi strains (*A. pullulans*) by chemical mutagenesis
- Characterized pullulan production on prairie cordgrass hydrolysate
- Present at Research Symposium sponsored by Sun Grant Initiative, Aug. 2012

Research Assistant; Penn State University, University Park, PA Spring 10 - Fall 13
Departments of Chemical Engineering and Biochemistry and Molecular Biology
Professors Janna Maranas and Craig E. Cameron

Interaction Networks in RNA-Dependent-RNA-Polymerase

- Cloned, purified, and analyzed poliovirus mutants for fidelity and kinetics
- Modeled the wild-type and mutant polymerase in AMBER MD
- Presented at Penn State Research Symposium, Aug. 2011

Research Assistant; Penn State University, the Behrend College, Erie, PA Fall 09 - Fall 10
Department of Biology

Professor Michael Campbell

Analysis of Non-Dormant Specific Genes in Potatoes and *Gene Expression Analysis in DMN-Treated Tissues*

- Evaluated and compiled extensive amounts of genetic data in Excel and R
- Analyzed gene expression levels of potatoes in a research team
- Experienced in PCR, gene isolation, and DNA sequencing

Association Memberships/Activities

- Undergraduate Assistant, *Cardiac Cares Medical Mission Trip*
- Secretary/Educational Outreach Chair, Engineers for a Sustainable World(ESW)
- Educational Outreach Chair, American Society of Chemical Engineers (AIChE)
- Educational Outreach Chair, Tau Beta Pi Engineering Honor Society
- Volunteer, Society of Women Engineers (SWE)
- Choreographer, Penn State International Dance Ensemble (PSIDE)
- Member, Biomedical Engineering Society (BMES)

Research Interests

I am interested in the combination of computational and experimental analysis and towards interdisciplinary questions in biomedical engineering and biology at the tissue to sub-cellular scale. With a broad range of previous research topics, I would like to apply new biological techniques to engineering applications.

Research Presentations

Senkow, T. L., J. L. Peterson and T. P. West. 2013. Isolation of fungal mutants exhibiting elevated pullulan production on hydrolyzed prairie cordgrass. 35th Symposium on Biotechnology for Fuels and Chemicals, Abstract 8-50, page 126, April 29-May 2, Portland, OR.

Senkow, Tiffany; West, Thomas. *Pullulan Production on Prairie Cordgrass Hydrolysate*. Presented at the South Dakota REU Research Symposium, Brookings, SD, Aug. 3, 2012.

Senkow, Tiffany; Farran. Maria; Cameron, Craig; Maranas, Janna. *Long Range Interaction Networks in RNA-Dependent-RNA-Polymerase*. Presented at the Pennsylvania State University REU Research Symposium, University Park, PA, Aug. 4, 2011.